
The development of highly sensitive carnitine biosensor based on cathodic stripping voltammetry

丹羽研究室

Zixin Zhang

(Doctoral Program in Life Science and Green Chemistry)

Dissertation submitted to the Graduate School of
Engineering in partial fulfillment of the requirements for the
degree of Doctor of Philosophy in Engineering at Saitama

Institute of Technology

Mar. 2021

Table of Contents

Table of Contents

CHAPTER 1. GENERAL INTRODUCTION	1
1.1 Introduction	1
1.2 Current study of carnitine	5
1.2.1 The function of carnitine in human body	5
1.2.2 Determination methods of carnitine	7
1.3 Self-assembled monolayers	15
1.4 Cathodic stripping voltammetry detection method- A electrochemistry technology	16
1.5 Purpose of this work	18
REFERENCES	20
CHAPTER 2. AU BULK ELECTRODE-BASED CARNITINE BIOSENSOR	
2.1 Introduction	27
2.2 Experimental section	30
2.2.1 Diagram of device	30
2.2.2 Reagents and materials	31
2.2.3 Apparatus	32
2.2.4 Enzyme immobilization	33
2.2.5 Linear-sweep cathodic stripping voltammetry analysis	34
2.3 Results and Discussion	35
2.3.1 Electrochemical behavior of CoA and acetyl-CoA on a bulk gold electrode	35
2.3.2 Optimization of enzyme membrane compositions of modified-gold bulk electrode	37
2.3.3 Optimization of enzyme membrane position on a gold bulk electrode	40
2.3.4 Carnitine calibration curves	42
2.3.5 Selectivity of carnitine biosensor	45
2.3.6 Recovery tests of spiked samples with carnitine in artificial saliva	46

Table of Contents

2.4 Conclusion	47
2.5 References	48
CHAPTER 3. THE STUDY OF SPUTTERED CARBON FILM FOR GOLD NANOPARTICLE-BASED BIOSENSOR	
3.1 Introduction	54
3.1.1 Carbon film	54
3.1.2 Metal nanoparticle modified carbon film electrode	56
3.2 Experimental section	59
3.2.1 Reagents and materials	59
3.2.2 Carbon film preparation	61
3.2.3 Gold nanoparticles electrodeposition	62
3.2.4 Carbon film characterization	63
3.2.5 Electrochemical measurements of pure carbon films	64
3.2.6 Cathodic stripping voltammetry analysis	65
3.3 Results and Discussion	66
3.3.1 Surface characterizations of DC sputter deposited carbon films	66
3.3.2 Potential windows of DC-sputtered carbon films	71
3.3.3 Basic electrochemical properties of DC carbon films	73
3.3.4 Optimization of AuNPs deposition parameters	79
3.3.5 Electrochemical behavior of CoA and acetyl-CoA on a AuNPs modified carbon film electrodes	83
3.3.6 Electrochemical behavior of carnitine biosensor	84
3.3.7 Carnitine calibration curves of AuNPs-based biosensor	86
3.3.8 Selectivity study of carnitine biosensor	88
3.3.9 Recovery in artificial saliva with carnitine biosensor based on AuNPs modified carbon film	89
3.4 Conclusion	90
3.5 References	92
CHAPTER 4. CONCLUSIONS	98
LIST OF ACHIEVEMENTS	101

Table of Contents

ACKNOWLEDGEMENT

103

Chapter 1. General Introduction

1.1 Introduction

Cancer has become one of the common diseases in daily life. According to the data of W.H.O (world health organization), it has become the second leading cause of death in human beings. In recent years, research data shows that cancer has a young trending with the rapid development of social economy and the accelerated pace of life.[1] Also, population aging has become a global trend. This information indicates that if we cannot pay attention to cancer in time, cancer will become a global catastrophe. Therefore, how to cure and prevent cancer is extremely important for future human life. Fig.1.1 shows the top 10 cancer death by type in Japan. It shows the fatality of lung cancer is much higher than other cancers. However, the sum of fatality number from the digestive system cancers (colon cancer, stomach cancer, pancreatic cancer, liver cancer, and gallbladder cancer) far exceeds lung cancer, suggesting that the digestive cancers are the most severe cancer in Japan.

In recent years, various cancer treatments have been developing based on improvement of the medical and biological technologies. The treatment given for cancer is variable and dependent on several factors, including the type, position, organs, cancer progression or size of the tumor, and the

Chapter 1.

health status of the patient. There are three general types of cancer treatments: radiation therapy, surgery, and systemic therapy. However, those treatments are only effective for early and mid-stage cancer patients. Hence, early detection of cancer becomes the key for treating and even preventing cancer.

The biomarkers in the human body can effectively and accurately reflect the health status of the human body. Therefore, invasion detection technology has been rapidly developed and applied to the early detection of cancer. However, the process of invasion detection often brings pain to the patient, which will cause many people to give up precious curable opportunities because of the pain during the detection process. In order to solve this problem, non-invasive detection methods came into being under the efforts of many researchers. Although the non-invasive detection method is not well-developed, some remarkable works have reported. For example, the biomarkers have been found in urine,[2] sweat[3-5] and saliva [6-8] samples.

Electrochemical methods were widely employed in biosensing applications and were usually combined with enzymatic or immunoassay to determine the biomolecules in the human body such as glucose, cholesterol, DNA, uric acid, lactate, hemoglobin, and others.[9-11] This is because the electrochemical measurements are highly sensitive, short-detection time, and easy-to-operate. Moreover, the target could be

Chapter 1.

quantitatively determined by electrochemical measurements despite of their inexpensive equipment. With the development of biosensing technology in recent years, biosensors have been successfully commercialized. And products have a trend of small size and simple operations, such as the smart-biochips shown in figure 1.2. Particularly the disposable sensor is essential for real clinical trials. Therefore, a suitable material is crucial for the development and fabrication of an ideal biosensor.

Carbon-based materials are widely used in electrochemical analysis due to their excellent electrochemical properties, such as low noise and good electrochemical stability. Many carbon electrode based biosensors have been developed by utilizing electrochemical technology, such as, glucose,[12-14] H_2O_2 [15, 16] and alcohol biosensors [17], as listed in Table 1.1. For realizing chip-shaped with carbon-based electrodes for the manufacture of biosensors, carbon films are mass-producible and can be fabricated with any shape and size. Therefore, we can achieve a promising disposable and non-invasive biosensors with small-size, accurate, and easy-to-operate using carbon films and electrochemical measurements.

Chapter 1.

Table. 1.1 The performance summary of the carbon-based biosensors

Method	Target	Performance	Linear range
CR-GO glucose sensor [12]	glucose	2.00 μM	0.01 to 10 mM
H-ERGO based sensor [15]	H_2O_2	8.33 μM	From 25 to 8850 and 8820 to 28850 μM
Graphene-based glucose biosensor [13]	glucose	2 mM	2 to 14 mM
CNT-Gox glucose sensor [14]	glucose	5 mM	up to 35 mM
CNT-Based Dehydrogenase Biosensor[17]	NADH	0.1 mM	1 to 5mM
CNT-Based Peroxidase biosensor[16]	H_2O_2	100 nM	0.3 to 200 μM

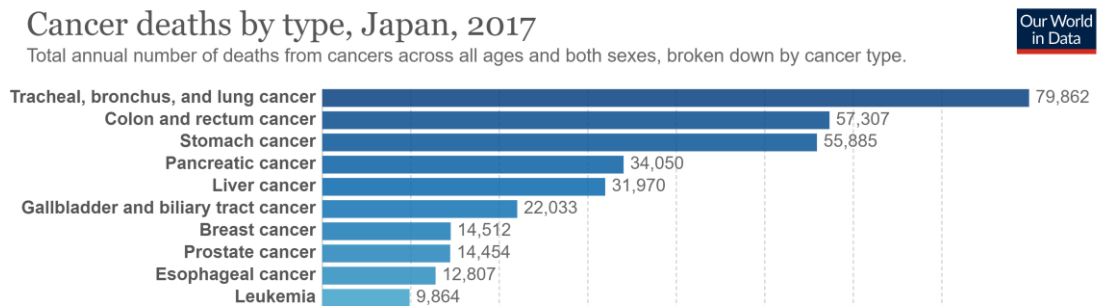


Figure 1.1 The top 10 cancer death by type in Japan, (2017).

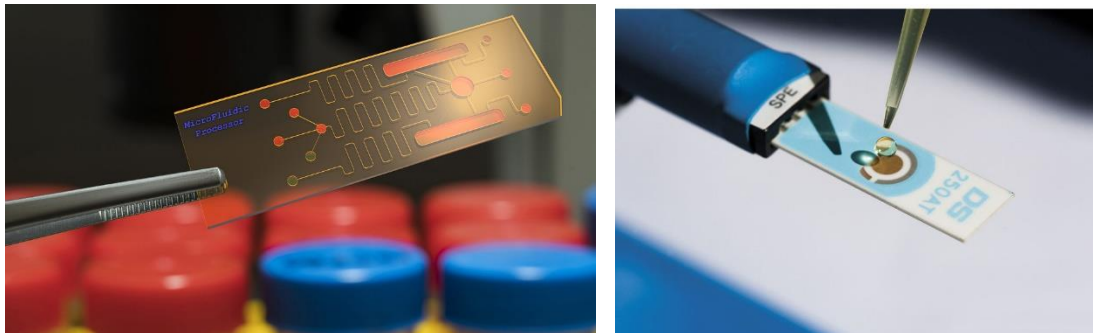


Figure 1.2 The figure of smart-chip-like biosensor.[18, 19]

1.2 Current study of carnitine

1.2.1 The function of carnitine in human body

Carnitine is a quaternary ammonium compound derived from an amino acid as shown in figure 1.3. It is mainly distributed in the digestive system and the liver, and is involved in the metabolism of fatty acids (Fig. 1.4). Carnitine also provides antioxidant and anti-inflammatory effects. Carnitine is commonly present in the mitochondria in a cell, where it helps to convert long-chain fatty acids to energy (e.g., ATP)[20], and approximately 75 % of carnitine found in the human body derives from our diet, and the remainder is synthesized from lysine and methionine in the liver and kidneys [21]. Carnitine can also transport any toxins that are produced to the mitochondria to prevent toxin accumulation [22]. In view of these key functions, carnitine will be concentrated in tissues such as bones and heart muscle, which use fatty acids as dietary fuel.

Also, L-carnitine deficiency is usually observed in chronic hemodialysis patients,[23] and researchers reported that the chronic fatigue syndrome,[24] methylmalonic acidemia,[25] and even heart failure and Alzheimer disease[26] might associate with the carnitine amount in the human body. Therefore, the carnitine was also considered as a confident evidence of human health status. Moreover, the carnitine in human saliva was reported as a pancreatic cancer biomarker. The amount of carnitine

Chapter 1.

found in cancer patients and healthy subjects were about 20 and 10 μM , respectively.[7]

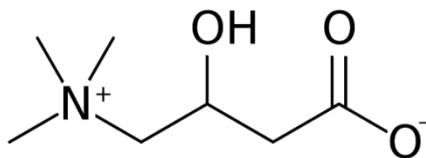


Figure 1.3 The chemical structure of carnitine.

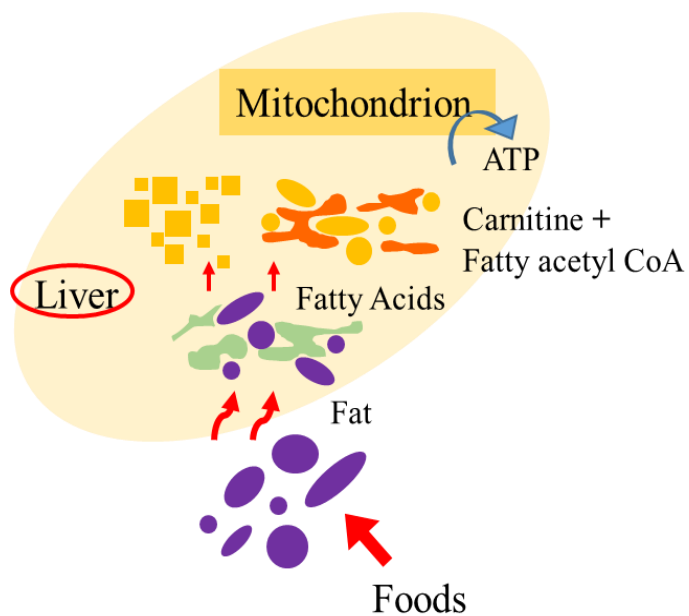


Figure 1.4 The function of carnitine.

Chapter 1.

1.2.2 Determination methods of carnitine

1.2.2.1 Traditional carnitine detection methods

High-performance liquid chromatography detection method

High-Performance Liquid Chromatography (HPLC) is an analytical chemistry technique used to separate and quantify each component in a mixture sample.

Minkler et al. utilized the HPLC method to detect the content of total carnitine and acetyl-carnitine in human urine and plasma. They successfully determined the relationship between the content of total carnitine and acetyl-carnitine in urine and methylmalonic aciduria, isovaleric acidemia, and medium chain acyl-CoA dehydrogenase deficiency. The carnitine and acetyl-carnitine were separated from urine using 0.5-ml columns of silica gel, and obtained a linear range of 10-300 nmol/mL. [27, 28] However, HPLC method is time-consuming and high-cost of equipment.



Figure 1.5 The HPLC system

High Performance Liquid Chromatography (HPLC)

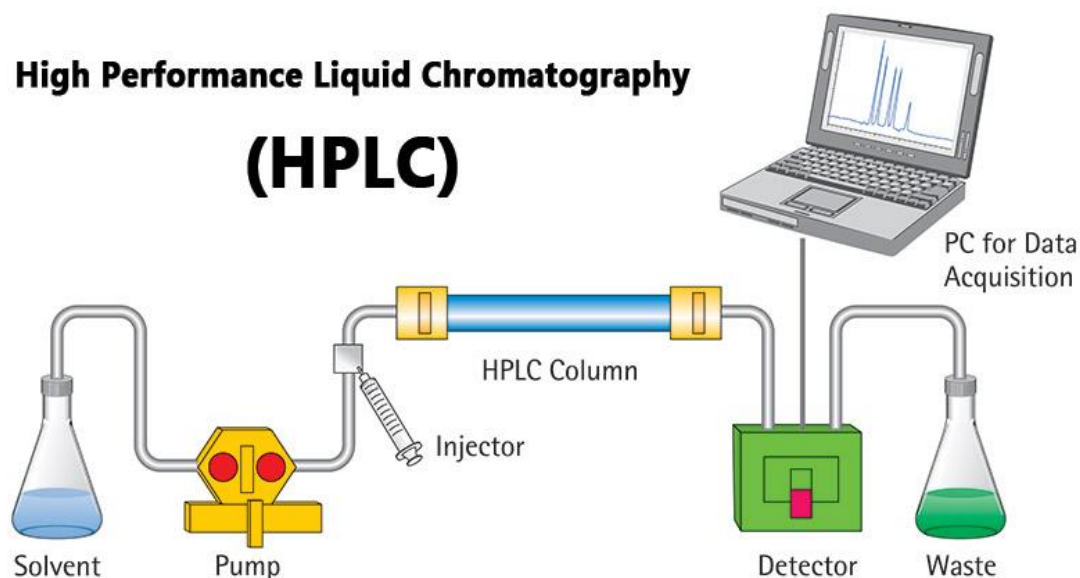


Figure 1.6 the schematic diagram of HPLC.[29]

Capillary electrophoresis mass spectrometry (CE-MS)

CE-MS is a technology which combined the capillary electrophoresis and mass spectrometry.

Heinig et al. reported the determination of carnitine and acylcarnitines in human urine and plasma samples by CE-MS. The separation of carnitine and acylcarnitines were performed in aqueous, mixed organic–aqueous and non-aqueous media by CE. To improve the separation efficiency, the electrolyte compositions were optimized. Then the separated carnitine and acylcarnitines were determined by MS. An acceptable performance with a linear range of 2.7 to 108 nmol/mL and a LOD of 12 nmol/mL was achieved.[30] Sánchez-Hernández et al. determine D-carnitine of the non-protein amino acid carnitine in 22 dietary food supplements. The D-

Chapter 1.

carnitine were separated by CE, and determined by an improved MS/MS method. As a result, an LOD of 10 ng/ml and detection ranged from 0.4 % and 5.9 % were obtained.[31]



Figure 1.7 CE/MS system

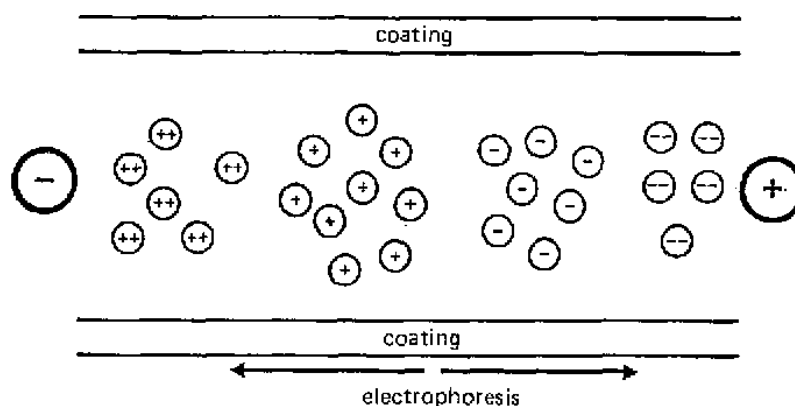


Figure 1.8 Schematic diagram of CE method.

Liquid chromatography mass spectrometry

Liquid chromatography-mass spectrometry (LC-MS) is an analytical chemical technique that combines the separation capabilities of liquid

Chapter 1.

chromatography (or HPLC) with the mass spectrometry (MS). Due to the synergistic enhancement of the respective functions of each technology, the combined chromatography-MS system is very popular in chemical analysis.

The free carnitine in milk-based infant formula and health-care products was determined by Andrieux et al. The free carnitine was separated by liquid chromatography and quantified by ion-pair chromatography with single-quadrupole MS detection. As a result, the intermediate reproducibility relative standard deviation and the average product-specific recoveries range were less than 4.7 and 92–98%, respectively. [32]

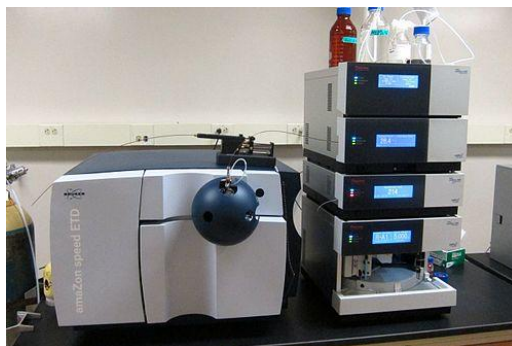


Figure 1.9 LC/MS system

Chapter 1.

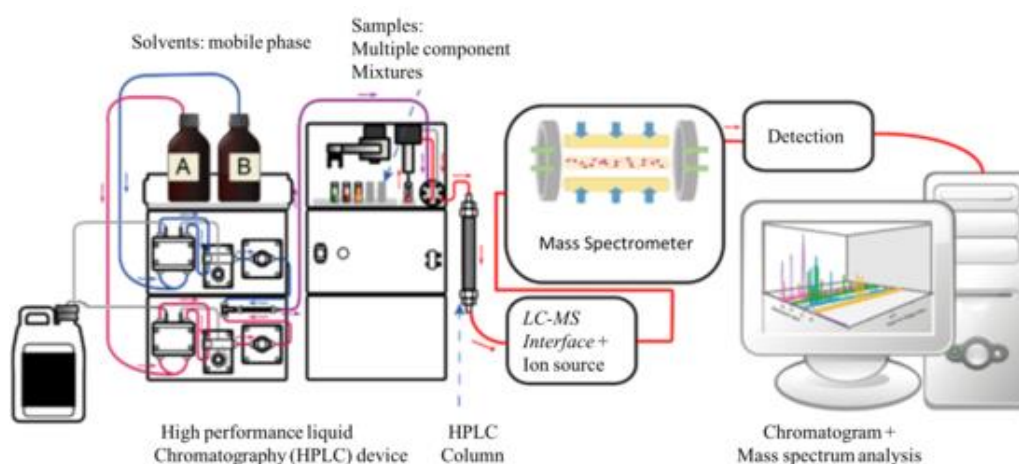


Figure 1.10 Schematic diagram of LC-MS.[33]

Radio-assay

The radioisotopic assay usually combines with the enzymatic assay by pre-labeling the ^{14}C isotope on the acetyl functional group. Carnitine concentration was quantified by determining the content of the isotopic. The enzymatic reaction was shown in figure 1.11.

Carnitine acetyltransferase

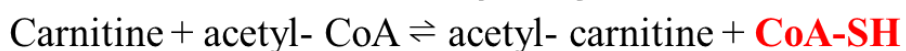


Figure 1.11 The enzymatic reaction of carnitine.

McGarry et al. reported an improved and simplified radioisotopic assay to determine free and total carnitine in human plasma samples. The plasma sample was incubated with a neutralized perchloric acid with [^{14}C]

Chapter 1.

acetyl-CoA. After the enzymatic reaction, the labeled acetyl-carnitine was separated by passing the mixture through a column of anion exchange resin. And the isotope content determined from the effluent fluid. As a result, 55.7 ± 1.99 and 65.7 ± 2.55 $\mu\text{M/L}$ of free carnitine and total carnitine were detected from human plasma samples, results which are in close agreement with those reported by others at that time. [34]

To sum it up, although the traditional carnitine detection methods have a good performance as shown in Table 1.2, the time-consuming and high-cost of equipment slow down the promotion of commercialization.

Table. 1.2 The performance of the traditional carnitine detection method.

Method	Performance (LOD)	Linear range	Detection time (min)	Reaction volume	Cost
HPLC (K. Li, Q. Sun.)	1 μM	5-400 (μM)	60	100 μL	High
CE-MS (K. Heinig, J. Henion,)	1.8 $\mu\text{g/ml}$	1.8-30 ($\mu\text{g/ml}$)	45	2 mL	High
LC-MS (L.S-Hernández, et al)	0.1 μM	0.1-1000 (μM)	10	20 μL	High
Radio-assay (K.-G. Seline, et al)	0.11 μM	0.11-15 (μM)	85	0.9 mL	High

Chapter 1.

1.2.2.2 Enzyme-based carnitine biosensor

Recently, an Ion-sensitive field-effect transistor (ISFET) based carnitine biosensor was reported by Andianova et al. [35] A new sensor based on specially optimized for biosensing (complementary metal-oxide-semiconductor) CMOS-compatible ISFET structures. The CMOS membrane (Ta_2O_5) was modified with an enzymatic membrane containing carnitine acetyltransferase for the direct determination of L-carnitine. The schematic diagram of this ISFET carnitine biosensor was shown in Fig. 1.12.

The CMOS structure was optimized for achieving high sensitivity using a subthreshold operation mode and by reducing the influence of the capacitances on the value of subthreshold swing. The developed ISFET was used as a basis for a biosensor for L-carnitine detection. The carnitine enzymatic products can change the pH values of solution, and the Ta_2O_5 film is very sensitive to the ionic charge. Therefore, the amount carnitine can be detected by the ISFET sensor. The detected L-carnitine at a range of 0.2–100 μM with a LOD of 0.2 μM . The biosensor response was linear in the range of 0.2–50 μM of L-carnitine with sensitivity $18.0 \pm 1.7 \text{ mV}/\mu\text{M}$.

Chapter 1.

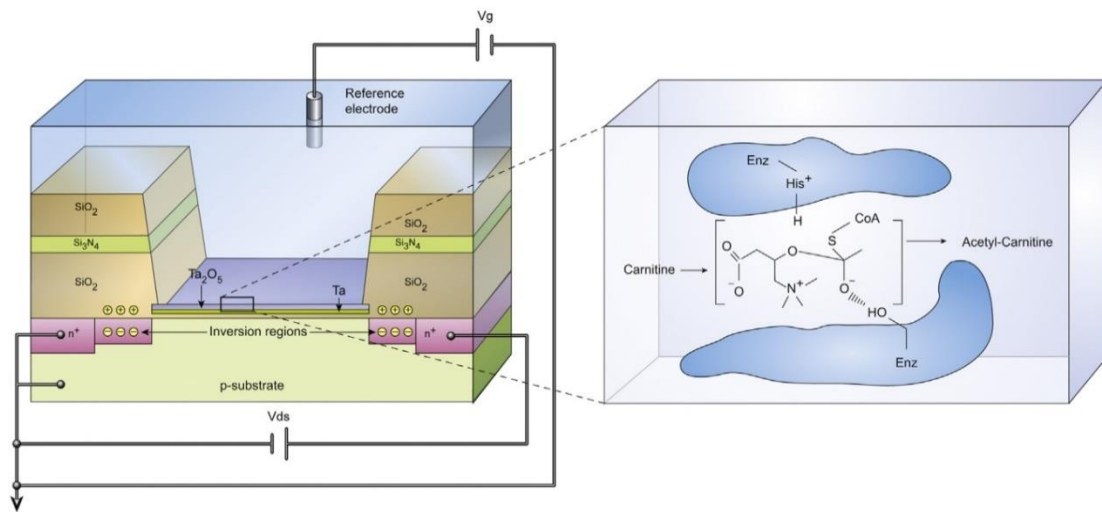


Figure 1.12 The schematic diagram of ISFET carnitine biosensor[35]

1.3 Self-assembled monolayers

SAM is an ordered molecular assembly formed by adsorbing active surfactants on a solid surface. This simple process makes SAM inherently manufacturable, and therefore technically attractive for superlattice construction and surface engineering. In these two-dimensional systems, when the system is in equilibrium, the spontaneous chemical synthesis at the interface produces a sequence.[36]

The CoA-**SH**, the carnitine enzymatic product, has a thiol-terminated functional group, which allows CoA-SH can easily adsorb on the surface of noble metals (*e.g.*, gold, silver, platinum) to form SAMs as shown in Fig. 1.13.

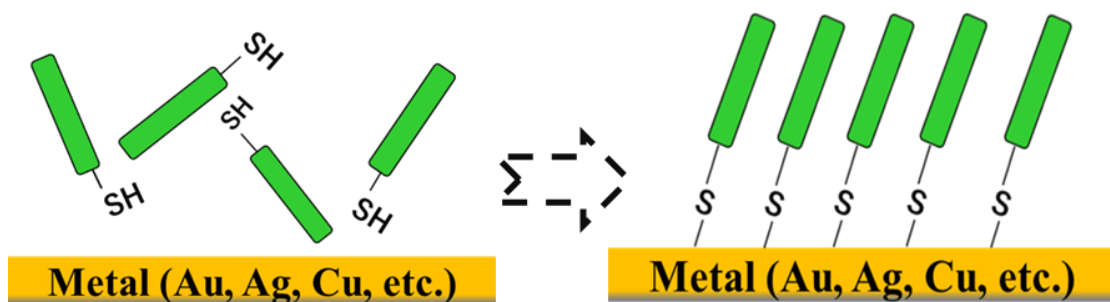


Figure 1.13 The pre-concentration of SAMs on the noble metal surface.

1.4 Cathodic stripping voltammetry detection method- A electrochemistry technology

Cathodic stripping voltammetry (CSV) has been used to identify metal types and quantify them based on their reduction current. CSV has a pre-concentration step, which usually involves adsorption of complexes with selective ligands (usually organic ligands) on the electrode. For SAMs, it is the formation of Au-S-R (Fig. 1.14). There is no diffusion during scanning, so a high scanning rate can be used to obtain high sensitivity. The sensitivity of CSV is sufficient to detect about 20 elements in seawater.[37]



Figure 1.14 The assumed formation of a gold–thiolate ligands.

By using this property, CSV could be utilized for thiol group determination. CSV has many advantages, such as high sensitivity, accuracy, and applicability to small volume samples. Moreover, in recent years, many researchers have used the CSV method to detect biomarkers, and have achieved very satisfactory results. As shown in the Table 1.3:

Table. 3 The application of CSV for determination.

Target	Technology	Performance	Linear range
Cardiac biomarker[38]	Enzyme-free electrochemical immunoassay	3.8 pg mL ⁻¹	0.01 to 500 ng mL ⁻¹
Metallothionein for evaluating environmental contamination[39]	Modified square wave CSV	5 × 10 ⁻⁸ g L ⁻¹	up to 100 ug*g ⁻¹
Cancer biomarker[40]	Stripping voltammetric immunoassay (SVI)	pg mL ⁻¹ level	1 to 50 ng*ml ⁻¹
Cardiac marker[41]	CSV-based electrochemical enzyme immunoassay system	20 ng L ⁻¹	20 and 40 ng L ⁻¹

1.5 Purpose of this work

In this study, we developed a highly sensitive carnitine biosensor by the CSV method using a gold electrode modified with an enzyme (carnitine acetyltransferase). The biosensor concentrates CoA produced by the enzymatic reaction of carnitine, acetyl coenzyme A (acetyl-CoA) and carnitine acetyltransferase on a gold electrode by a self-assembling reaction, and electrochemically reduces it all at once, resulting in a large current. A signal can be obtained and a low detection limit can be achieved. Both acetyl-CoA and CoA are adsorbed on the gold electrode, but CoA is selectively detected by the potential difference of reduction elimination.

We first constructed a biosensor based on a commercially available gold electrode and achieved a detection limit of 0.025 μM (Chapter. 2). In order to further improve the performance, AuNPs deposited sputtered carbon film electrode was employed in further biosensor development study. Because the substrate of AuNPs could extremely affect the electrochemical properties of biosensor. Therefore, we studied the DC magnetron sputtered carbon film first, the electrochemical properties and the structures were characterized by cyclic voltammetry (CV), XPS, and TEM. Then, we developed a new electrode modified with gold nanoparticles, the AuNPs deposition conditions were evaluated by the reduction peak obtained by CV in sulfuric acid aqueous solution. And the

Chapter 1.

performances of biosensor were evaluated by the reduction peak obtained by SWCSV in potassium hydroxide aqueous solution (Chapter. 3).

References

[1] K.D. Miller, M. Fidler-Benaoudia, T.H. Keegan, H.S. Hipp, A. Jemal, R.L. Siegel, Cancer statistics for adolescents and young adults, 2020, CA: A Cancer Journal for Clinicians, 70(2020) 443-59.

[2] B.W. van Rhijn, H.G. van der Poel, T.H. van der Kwast, Urine markers for bladder cancer surveillance: a systematic review, European urology, 47(2005) 736-48.

[3] V. Oncescu, D. O'Dell, D. Erickson, Smartphone based health accessory for colorimetric detection of biomarkers in sweat and saliva, Lab on a Chip, 13(2013) 3232-8.

[4] S. Jadoon, S. Karim, M.R. Akram, A. Kalsoom Khan, M.A. Zia, A.R. Siddiqi, et al., Recent Developments in Sweat Analysis and Its Applications, International Journal of Analytical Chemistry, 2015(2015) 164974.

[5] J. Choi, A.J. Bandodkar, J.T. Reeder, T.R. Ray, A. Turnquist, S.B. Kim, et al., Soft, Skin-Integrated Multifunctional Microfluidic Systems for Accurate Colorimetric Analysis of Sweat Biomarkers and Temperature, ACS Sensors, 4(2019) 379-88.

[6] E. Kaufman, I. Lamster, Analysis of saliva for periodontal

Chapter 1.

diagnosis – a review [In Process Citation], *Journal of clinical periodontology*, 27(2000) 453-65.

[7] M. Sugimoto, D.T. Wong, A. Hirayama, T. Soga, M. Tomita, Capillary electrophoresis mass spectrometry-based saliva metabolomics identified oral, breast and pancreatic cancer-specific profiles, *Metabolomics*, 6(2010) 78-95.

[8] A.E. Herr, A.V. Hatch, D.J. Throckmorton, H.M. Tran, J.S. Brennan, W.V. Giannobile, et al., Microfluidic immunoassays as rapid saliva-based clinical diagnostics, *Proceedings of the National Academy of Sciences of the United States of America*, 104(2007) 5268-73.

[9] Z. Guler, P. Erkok, A.S. Sarac, Electrochemical impedance spectroscopic study of single-stranded DNA-immobilized electroactive polypyrrole-coated electrospun poly(ϵ -caprolactone) nanofibers, *Materials Express*, 5(2015) 269-79.

[10] Y. Wang, H. Xu, J. Zhang, G. Li, Electrochemical Sensors for Clinic Analysis, *Sensors*, 8(2008) 2043-81.

[11] M.B. Akolpoglu, U. Bozuyuk, P. Erkok, S. Kizilel, Chapter 9 - Biosensing–Drug Delivery Systems for In Vivo Applications, in: Inamuddin, R. Khan, A. Mohammad, A.M. Asiri (Eds.), *Advanced Biosensors for Health Care Applications*,

Chapter 1.

Elsevier2019, pp. 249-62.

[12] M. Zhou, Y. Zhai, S. Dong, Electrochemical Sensing and Biosensing Platform Based on Chemically Reduced Graphene Oxide, *Anal Chem*, 81(2009) 5603-13.

[13] C. Shan, H. Yang, J. Song, D. Han, A. Ivaska, L. Niu, Direct Electrochemistry of Glucose Oxidase and Biosensing for Glucose Based on Graphene, *Anal Chem*, 81(2009) 2378-82.

[14] J. Wang, M. Musameh, Enzyme-dispersed carbon-nanotube electrodes: a needle microsensor for monitoring glucose, *The Analyst*, 128(2003) 1382-5.

[15] Z. Chen, D. Liu, C. Zhu, L. Li, T. You, Facile Preparation of Hemin-functionalized Electrochemically Reduced Graphene Oxide Nanocomposite for H₂O₂ Biosensing, *Sensors and Materials*, 31(2019) 1167.

[16] K. Yamamoto, G. Shi, T. Zhou, F. Xu, J. Xu, T. Kato, et al., Study of carbon nanotubes–HRP modified electrode and its application for novel on-line biosensors, *The Analyst*, 128(2003) 249-54.

[17] J. Wang, M. Musameh, A Reagentless Amperometric Alcohol Biosensor Based on Carbon-Nanotube/Teflon Composite Electrodes, *Anal Lett*, 36(2003) 2041-8.

[18] Biosensors in medicine.

Chapter 1.

- [19] Biosensors: sensing elements and techniques.
- [20] J. Bremer, Carnitine--metabolism and functions, *Physiological Reviews*, 63(1983) 1420-80.
- [21] C.J. Rebouche, Quantitative estimation of absorption and degradation of a carnitine supplement by human adults, *Metabolism*, 40(1991) 1305-10.
- [22] R.-I. Stefan, R.G. Bokretsiou, J.F. van Staden, H.Y. Aboul-Enein, Biosensors for the Determination of Ortho-acetyl-L-carnitine. Their Utilization as Detectors in a Sequential Injection Analysis System, *Preparative Biochemistry & Biotechnology*, 33(2003) 163-72.
- [23] T. Sakurabayashi, S. Miyazaki, Y. Yuasa, S. Sakai, M. Suzuki, S. Takahashi, et al., L-Carnitine Supplementation Decreases the Left Ventricular Mass in Patients Undergoing Hemodialysis, *Circulation Journal*, 72(2008) 926-31.
- [24] A.V. Plioplys, S. Plioplys, Serum Levels of Carnitine in Chronic Fatigue Syndrome: Clinical Correlates, *Neuropsychobiology*, 32(1995) 132-8.
- [25] F. Hörster, G.F. Hoffmann, Pathophysiology, diagnosis, and treatment of methylmalonic aciduria—recent advances and new challenges, *Pediatric Nephrology*, 19(2004) 1071-4.
- [26] A. Evangelidou, D. Vlassopoulos, Carnitine Metabolism

Chapter 1.

and Deficit - When Supplementation is Necessary?, *Current Pharmaceutical Biotechnology*, 4(2003) 211-9.

[27] P.E. Minkler, C.L. Hoppela, Determination of free carnitine and 'total' carnitine in human urine: derivatization with 4'-bromophenacyl trifluoromethanesulfonate and high performance liquid chromatography, *Clin Chim Acta*, 212(1992) 55-64.

[28] P.E. Minkler, C.L. Hoppel, Quantification of Free Carnitine, Individual Short- and Medium-Chain Acylcarnitines, and Total Carnitine in Plasma by High-Performance Liquid Chromatography, *Anal Biochem*, 212(1993) 510-8.

[29] High-Performance Liquid Chromatography (HPLC).

[30] K. Heinig, J. Henion, Determination of carnitine and acylcarnitines in biological samples by capillary electrophoresis-mass spectrometry, *Journal of Chromatography B: Biomedical Sciences and Applications*, 735(1999) 171-88.

[31] L. Sánchez-Hernández, M. Castro-Puyana, C. García-Ruiz, A.L. Crego, M.L. Marina, Determination of l- and d-carnitine in dietary food supplements using capillary electrophoresis-tandem mass spectrometry, *Food Chem*, 120(2010) 921-8.

Chapter 1.

[32] P. Andrieux, T. Kilinc, C. Perrin, E. Campos-Giménez, Simultaneous determination of free carnitine and total choline by liquid chromatography/mass spectrometry in infant formula and health-care products: Single-laboratory validation, *J AOAC Int*, 91(2008) 777-85.

[33] Liquid chromatography–mass spectrometry.

[34] J.D. McGarry, D.W. Foster, An improved and simplified radioisotopic assay for the determination of free and esterified carnitine, *J Lipid Res*, 17(1976) 277-81.

[35] M.S. Andrianova, E.V. Kuznetsov, V.P. Grudtsov, A.E. Kuznetsov, CMOS-compatible biosensor for L-carnitine detection, *Biosens Bioelectron*, 119(2018) 48-54.

[36] A. Ulman, Formation and Structure of Self-Assembled Monolayers, *Chem Rev*, 96(1996) 1533-54.

[37] E.P. Achterberg, C. Braungardt, Stripping voltammetry for the determination of trace metal speciation and in-situ measurements of trace metal distributions in marine waters, *Anal Chim Acta*, 400(1999) 381-97.

[38] B. Zhang, Y. Zhang, W. Liang, B. Cui, J. Li, X. Yu, et al., Nanogold-penetrated poly(amidoamine) dendrimer for enzyme-free electrochemical immunoassay of cardiac biomarker using cathodic stripping voltammetric method, *Anal*

Chapter 1.

Chim Acta, 904(2016) 51-7.

[39] W. Fan, X. Wang, X. Li, F. Xue, Determination of metallothionein in *Daphnia magna* by modified square wave cathodic stripping voltammetry, *Electrochem Commun*, 52(2015) 17-20.

[40] D. Wang, N. Gan, J. Zhou, P. Xiong, Y. Cao, T. Li, et al., Signal amplification for multianalyte electrochemical immunoassay with bidirectional stripping voltammetry using metal-enriched polymer nanolabels, *Sensors and Actuators B: Chemical*, 197(2014) 244-53.

[41] H. Matsuura, Y. Sato, O. Niwa, F. Mizutani, Electrochemical Enzyme Immunoassay of a Peptide Hormone at Picomolar Levels, *Anal Chem*, 77(2005) 4235-40.

Chapter 2. Au bulk electrode-based carnitine biosensor

2.1 Introduction

Carnitine is a quaternary ammonium compound derived from amino acids. It is mainly distributed in the digestive system, especially the liver, and participates in the metabolism of fatty acids, and provides antioxidant and anti-inflammatory effects. Carnitine is usually present in the mitochondria of cells and it can help convert fatty acids into energy (such as ATP).[1] About 75% of the carnitine in the human body comes from our diet, and the rest is synthesized in the liver by lysine and methionine in the kidneys.[2] Carnitine can also transport any toxins produced to the mitochondria to prevent the accumulation of toxins.[3] Salivary carnitine content has been reported as strong evidence for confidence in assessing health status and pancreatic cancer biomarkers. The carnitine levels found in cancer patients and healthy subjects are approximately 20 and 10 μM , respectively.[4]

Carnitine has been detected using traditional analytical methods such as high-performance liquid chromatography (HPLC)[5-10]. Capillary electrophoresis-mass spectrometry (CE-MS),[11, 12] HPLC-MS [13, 14] and gas chromatography (GC)-MS [15, 16] have been adopted because of their high sensitivity and reliability. However, these methods are time-

Chapter 2.

consuming and cause high equipment costs. Radioactivity and fluorescence measurements are also very accurate and reliable. However, the processing of radioisotopes requires special facilities and sufficient skills.[17-20] Although the fluorescence method combined with the enzymatic reaction shows a lower detection limit, the enzymatic reaction product should have absorbance in the UV/VIS range and have a higher fluorescence quantum yield.[21, 22]

Recently, by using complementary metal-oxide semiconductors (CMOS) compatible with Ta₂O₅ sensitive surfaces, enzyme sensors based on field-effect transistors (FET) have been developed.[23] In this method, carnitine acetyltransferase is immobilized on the surface of the FET, and the author speculates that in the presence of coenzyme A (CoA), the enzymatic reaction of carnitine may cause local pH changes on the surface of the Ta₂O₅ gate. However, the performance (such as detection limit) of FET-based carnitine sensors has not reached the level required for clinical applications. The above background indicates the need for an inexpensive carnitine biosensor with high sensitivity and short analysis time. Cathodic stripping voltammetry (CSV) has many advantages, such as high sensitivity, high accuracy, and suitability for small-volume samples. Many researchers have employed the CSV method to determine various biomolecules, including a cardiac biomarker by using enzyme-free electrochemical immunoassay,[24] a biomarker (metallothionein) for

Chapter 2.

evaluating environmental contamination by using modified square wave CSV,[25] a cancer biomarker by using stripping voltammetric immunoassay (SVI) to amplify the signal,[26] and a cardiac marker by using a CSV-based electrochemical enzyme immunoassay system.[27] In the former study, the performance of the detection limit can reach the pg level, which indicates that CSV technology might be very suitable for the determination of trace-level biomarkers.

In this work, the author developed a carnitine biosensor that combines the CSV method and enzymatic reaction. In this study, carnitine acetyltransferase converts carnitine and acetyl-coenzyme A (acetyl-coenzyme A) into acetyl-carnitine and coenzyme A (CoA). The CoA produced by the enzymatic reaction is a thiol compound that can be pre-concentrated on the surface of precious metals, including gold and silver. CSV can detect this pre-concentrated thiol compound by electrochemical methods with high sensitivity and low detection limit.[27] Although acetyl-CoA is also a thiol compound, the author found that CSV can selectively detect CoA by using the different reduction potential between acetyl-CoA and CoA. By optimizing parameters such as the amount of enzymes, low detection limits below the μM level can be achieved, and CSV parameters and methods have been successfully used to detect carnitine in artificial saliva samples. A recovery experiment was also successfully performed on artificial saliva samples.

2.2 Experimental section

2.2.1 Diagram of device

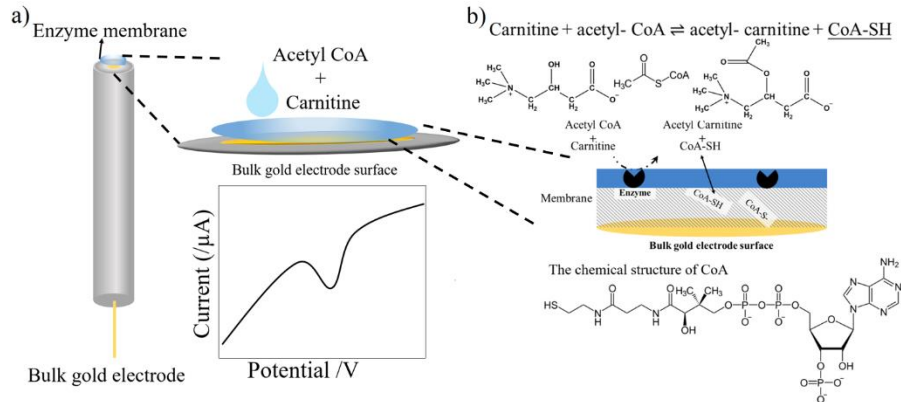


Figure 2.1. Schematic diagram of carnitine biosensor

Figure 2.1 shows a schematic diagram of the developed carnitine biosensor. The role of the BSA membrane with immobilized enzymes includes maintaining the activity of the enzyme and allowing carnitine and acetyl-CoA to react almost completely before reaching the electrode surface. When carnitine and acetyl-CoA react with the enzymes in the membrane, CoA and acetyl carnitine are produced, and coenzyme A accumulates on the surface of the gold electrode.

2.2.2 Reagents and materials

Bovine serum albumin (BSA) was obtained from Jackson ImmunoResearch Laboratories, Inc. (Pennsylvania, USA). Acetyl coenzyme A lithium salt (acetyl-CoA, enzymatic $\geq 93\%$) and carnitine acetyltransferase (40 unit/g) were purchased from Sigma-Aldrich (Tokyo, Japan). L-Carnitine was purchased from Fujifilm (Japan, Osaka). Glutaraldehyde (G.A.) 50 % (5 mM) water solution was purchased from KISHIDA CHEMICAL Co., Ltd. (Osaka, Japan). The artificial saliva used for the recovery experiment was purchased from Teijin (Tokyo, Japan), and composition is 14.44 μM NaCl, 16.11 KCl, 0.99 μM $\text{CaCl}_2 \cdot 2\text{H}_2\text{O}$, 0.55 μM MgCl_2 , and 1.96 μM K_2HPO_3 . Glucose, creatine, and urea were used as the interfering factors spiked in the artificial saliva for the selectivity studies, and glucose and creatine were purchased from Sigma-Aldrich (Tokyo, Japan) and urea was purchased Fujifilm (Japan, Osaka), respectively. The following buffer solutions were used: 0.1 M acetic acid buffer was used as the acetyl-CoA buffer. 0.1 M PB buffer (pH = 7.9) was used as the carnitine buffer, and the final pH of mixing buffers was 7.2.

2.2.3 Apparatus

An electrochemical analyzer (ALS model 720E BAS Co. Ltd., Tokyo, Japan) was used for the electrochemical measurements including CSV. A gold electrode ($d = 1.6$ mm BAS Co. Ltd., Tokyo, Japan), Ag/AgCl (RE-3V BAS Co. Ltd., Tokyo, Japan) and Pt wire were used as working, reference and counter electrodes, respectively. The electrolyte solutions (0.5 M KOH) were deoxygenated by purging them with pure Ar gas for 20 mins before the CSV measurements.

2.2.4 Enzyme immobilization

First, the author prepared the BSA and enzyme solutions separately. The range of BSA concentrations are between 0.6 and 1.8 μM , and the enzyme concentrations are ranged between $1 * 10^4$ to $5 * 10^4$ unit/g. Then after mixing the final concentrations of enzyme and BSA were ranged from $0.5 * 10^4$ to $2.5 * 10^4$ unit/g, and 0.3 to 0.9 μM , respectively. The same volumes of enzyme-BSA solutions were then mixed with different concentrations of GA solutions. The concentrations of GA solutions were ranged from 0.4 to 1.5 %, and the final concentrations were from 40 to 150 μM . After the mixing completed, 4 μL of the enzyme-BSA-GA solution was cast onto the gold electrode. The electrode was ready for experiments after the enzyme membrane had dried.

2.2.5 Linear-sweep cathodic stripping voltammetry analysis

Linear-sweep cathodic stripping voltammetry (LSCSV) was performed with an enzyme-modified gold bulk electrode. Before the LSCSV measurement, the author prepared a 20 μL solution containing 500 nM carnitine and 500 nM acetyl-CoA and incubated it with the enzyme-modified electrode for 30 min. Then, the electrode was rinsed with deionized water. After rinsing, the electrode was immersed in a 0.5 M KOH solution for an LSCSV measurement. The working electrode potential was scanned from -0.8 to -1.4 V at a scan rate of 0.05 V/s to observe the reductive desorption peak of CoA, which is correlated with the carnitine concentration

2.3 Results and Discussion

2.3.1 Electrochemical behavior of CoA and acetyl-CoA on a bulk gold electrode

Since CoA has a thiol group that can be adsorbed on the Au surface, acetyl-CoA has a thioester structure, which seems difficult to adsorb on the gold surface. However, previous literature reported that similar groups could strongly adsorb gold particles.[28, 29] Another literature also reported that chemicals with thioester groups could be electrochemically reduced on the electrode.[30] Therefore, it is essential to study the electrochemical reduction behavior of CoA and acetyl-CoA on Au bare electrodes. Figure 2.2 shows the LSCSV curves of CoA and acetyl CoA at different concentrations from 500 nM to 10 μ M. The reduction peaks of CoA and acetyl CoA were observed at -1.2 and -1.0 V, respectively.

In Fig. 2.2, no response was observed without CoA and acetyl-CoA, suggesting no interference from the chemicals used for buffer solutions. The reduction peak of CoA was about 200 mV lower than that of acetyl-CoA. These results indicated that CoA could be detected selectively against acetyl-CoA thanks to the different reduction potentials of acetyl-CoA and CoA, although both CoA and acetyl-CoA adsorb on the gold electrode. The currents from 0 to 1 μ M for both CoA and acetyl-CoA exhibited increases dependent on their concentrations, but the current for 10 μ M was very

Chapter 2.

small when the high concentration is taken into account, suggesting that the adsorption on the flat Au electrode surface saturates. This indicates that a quantitative evaluation of CoA could be possible for a lower CoA concentration range.

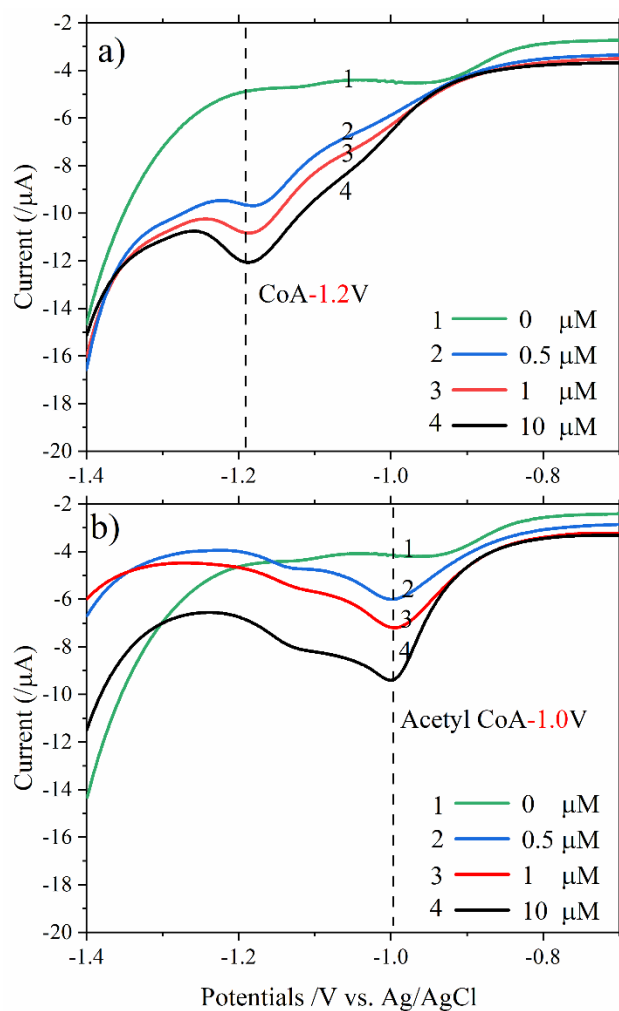


Figure 2.2. LSCSV curves of different CoA and acetyl-CoA concentrations with a gold electrode. (a: Different CoA concentrations; b: different acetyl-CoA concentrations; Electrolyte: 0.5 M KOH solution, scan rate: 0.05 V/s)

2.3.2 Optimization of enzyme membrane compositions of modified-gold bulk electrode

To achieve high sensitivity, the author optimized the composition of the enzyme membrane, as shown in Figure 2.3. Before the optimization study, the author checked the response of the buffer and different modified materials on the bare gold electrode. However, no response was observed at bare Au electrode after modifying membrane materials including BSA, GA, BSA+GA BSA+GA+enzyme. Figure 2.3(a) shows the relationship between the BSA concentration and the LSCSV curve, where the concentration of enzyme and GA are fixed at 4 % (or 1.0×10^4 U/g) and 0.5 %, respectively. A prominent peak of CoA was observed with 0 % BSA. However, a more pronounced acetyl-CoA peak was also observed. If the electrode is used continuously, the direct cross-linking of the enzyme and GA will reduce the enzyme activity.

When the BSA concentration was increased, the CoA peak was still clearly observed up to a BSA concentration of 1 %. However, the CoA peak decreased with a further increase in BSA concentration. This might be because the enzyme film is too thick, or some parts of the BSA and enzyme were dissolved in the solution due to insufficient GA. In contrast, when the CoA peak was maintained at a BSA concentration of about 1 %, the acetyl

Chapter 2.

CoA reduction peak was significantly suppressed. This result indicates that acetyl-CoA diffusion to the Au surface can be inhibited by consuming acetyl-CoA in the enzyme membrane. Therefore, the concentration of BSA was fixed to 1 % for further experiments. Figure 2.3(b) shows the change of the LSCSV curve when the enzyme concentration changes. When the fixed BSA and GA concentrations are 1 and 0.5 %, respectively, the enzyme concentration range is 2 % to 10 % (the final concentration range is 0.5×10^4 to 2.5×10^4 U/g). Both acetyl-CoA and CoA peaks were observed when the enzyme concentration was below 4 %, but the CoA peak was slightly smaller than those at higher enzyme concentrations of 8 and 10 %. The acetyl-CoA peak disappeared at a higher enzyme concentration, indicating that the enzymatic reaction is a rate determined step when the enzyme concentration is lower than 4 %. This also indicates that the acetyl-CoA diffused into the enzyme membrane is mainly consumed by the enzyme reaction before reaching the Au electrode surface, thereby enhancing the selective adsorption of CoA on the electrode surface. Therefore, the author chose an enzyme concentration of 10% to achieve a complete enzymatic reaction. Figure 2.3(c) shows the change of the LSCSV curve as the GA concentration increases. The concentration of BSA and enzyme were 1 % and 10 %, respectively, and the concentration of GA increased from 0.2 % to 0.75 %. At lower GA concentrations, both acetyl CoA and CoA peaks were observed. In contrast, only a CoA peak

Chapter 2.

could be observed when the GA concentrations were 0.5 or 0.6 %, suggesting that the GA concentration was sufficient to immobilize the enzyme in the membrane. However, when the GA concentration further increased to 0.75 %, the acetyl-CoA peak appeared again, suggesting that the enzymatic reaction rate was reduced as a result of the deactivation of the enzyme by GA. Therefore, the mild crosslink reaction condition of the 0.5 % GA concentration was selected to maintain enzyme activity and high sensitivity.

As summarized above, the author have optimized an enzyme membrane composition consisting of 1 % BSA, 10 % (or 2.5×10^4 U/g) enzyme, and 0.5 % glutaraldehyde.

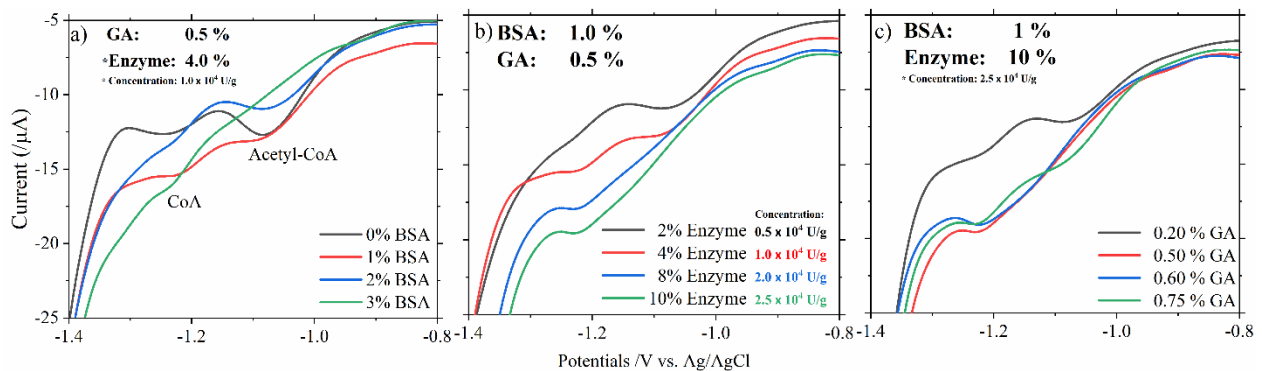


Figure 2.3. Optimization of BSA, enzyme, and glutaraldehyde (GA) concentrations in the enzyme membrane. (a. Different BSA solution concentrations; b. Different enzyme concentrations; c. Different GA concentrations; Sample solution: PB buffer mixing with acetate buffer (pH= 7.2) containing 500 nM carnitine, and 500 nM acetyl-CoA), Electrochemical desorption: in pH 13.5, Scan rate: 50 mV/s.

2.3.3 Optimization of enzyme membrane position on a gold bulk electrode

To achieve high sensitivity, the amount of enzymatically produced CoA diffused to the surface of the Au electrode is very important. Therefore, the author studied the dependence of the position of the enzyme membrane on the coenzyme A reduction peak produced by the enzymatic reaction of carnitine and acetyl-CoA. Figure 2.4 shows the LSCSV results of the enzyme membrane composition, composed of 1 % BSA, 0.5 % GA, and 10 % (or 2.5×10^4 U/g) carnitine acetyltransferase. The enzyme membrane was modified by surrounding the Au electrode with a membrane or directly on the electrode. When the enzyme membrane surrounds the Au electrode, reduction peaks are observed at -1.25 and -1.04 V, which belong to CoA and acetyl-CoA, respectively. However, the reduction peak of CoA is significantly smaller than the peak of acetyl-CoA, indicating that the enzyme membrane position is inappropriate. This might be because the diffusion distance of the produced CoA greatly exceeds the diffusion distance of the acetyl CoA already existing near the surface of the Au electrode. Due to the long diffusion distance to the Au electrode surface, some parts of the generated CoA might diffuse into the bulk solution. In contrast, only the CoA reduction peak was observed near -1.23 V when the

Chapter 2.

enzyme membrane was directly modified on the Au electrode surface. This indicates that most of the acetyl-CoA molecules diffused into the enzyme membrane might be converted into CoA before reaching the surface of the Au electrode, thereby increasing the sensitivity and selectivity of carnitine. Based on the above results, the author directly modified the enzyme membrane on the Au electrode to evaluate the sensitivity and detection limit.

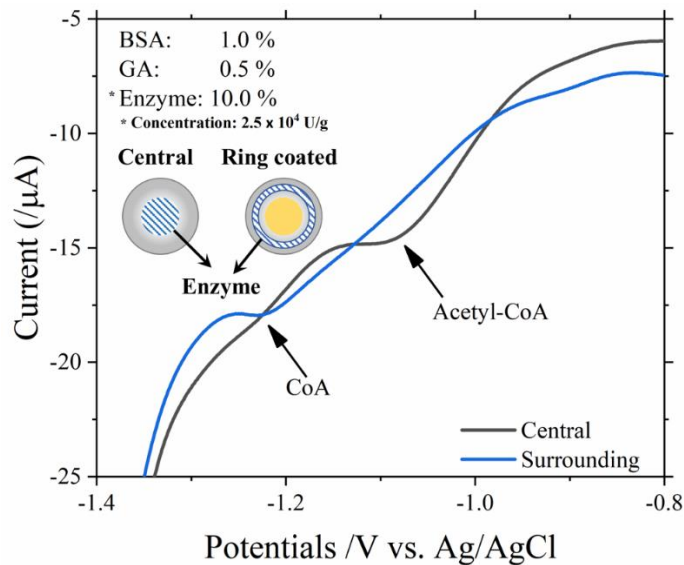


Figure 2.4. Comparison of modified enzyme membrane positions for carnitine determination. (Sample solution: PB buffer (pH= 7.9) containing 500 nM carnitine, and cofactor(acetyl-CoA) solution: acetic acid buffer (pH= 5.0) 500 nM acetyl-CoA; the final pH of buffer solution: 7.2) Electrochemical desorption: in pH 13.5, Scan rate: 50 mV/s.

2.3.4 Carnitine calibration curves

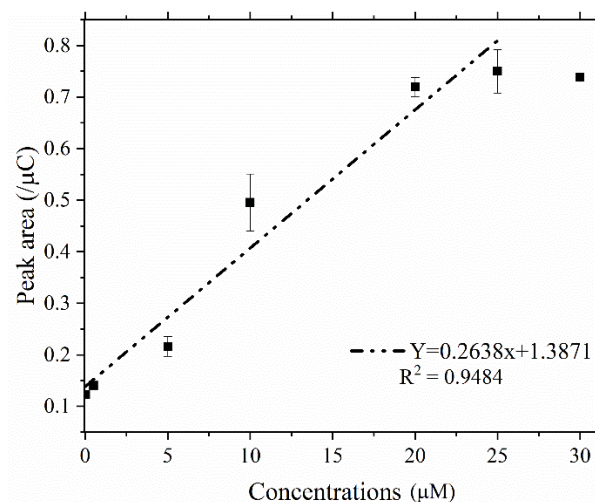


Figure 2.5. Relationship between CoA reduction current and carnitine concentration.

The relationship between the CoA reduction current and the carnitine concentration was obtained, as shown in Fig. 2.5. The obtained linear range for carnitine from 0.025 to 25 µM where the linear regression equation is $Y(-10^{-7}C) = 0.2638x + 1.3871$ ($R^2 = 0.9484$). However, the peak current was almost saturated when the carnitine concentration exceeded 25 µM, which might be due to the limit of the enzyme reaction or the saturation of the CoA adsorption. In the latter case, the calibration curve could be obtained in a higher concentration region by reducing the incubation time for the enzymatic reaction.

The calculated detection limit was 0.025 µM ($S/N = 3$), which is lower

Chapter 2.

than the previously reported values (Table 2.1). Our sensor requires a much lower equipment cost with an acceptable detection time. The employment of mass reproducible working electrodes such as Au film electrodes or carbon electrodes modified or embedded with Au nanoparticles that previously reported might greatly reduce the chip cost.[31] Although the FET sensor is also inexpensive and offers a shorter detection time, our sensor is more advantageous in that it has a detection limit that is about one order lower, making it suitable for real sample measurements.

Table 2.1. Comparison of analytic performance of different carnitine determination methods.

Method	Performance (LOD)	Linear range	Detection time (min)	Reaction volume	Cost
HPLC[10]	1 μ M	5-400 (μ M)	60	100 μ L	High
CE-MS [11]	1.8 μ g/ml	1.8-30 (μ g/ml)	45	2 mL	High
LC-MS [14]	0.1 μ M	0.1-1000 (μ M)	10	20 μ L	High
Radio-assay [20]	0.11 μ M	0.11-15 (μ M)	85	0.9 mL	High
FET-biosensor [23]	0.2 μ M	0.2-100 (μ M)	10	2 μ L	Relatively low
This work	0.025 μ M	0.025-25 (μ M)	30	20 μ L	low

2.3.5 Selectivity of carnitine biosensor

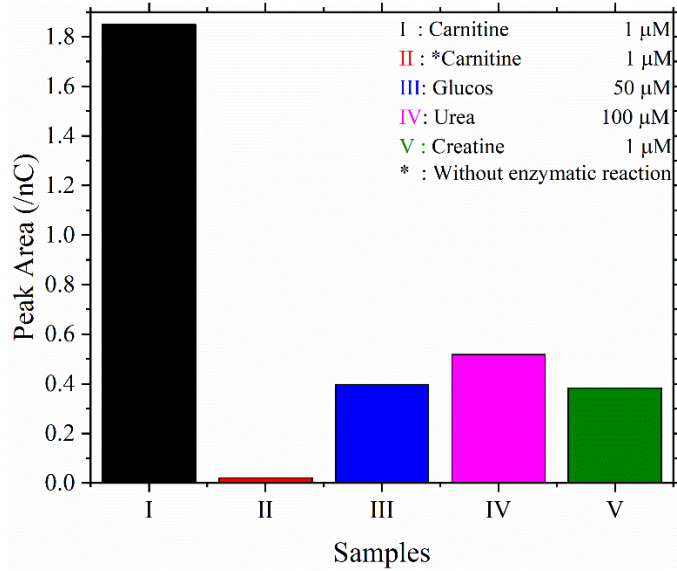


Figure 2.6. Selectivity studies with possible interferences.

For selectivity study, three interfering factors in saliva were spiked in artificial saliva, namely glucose, urea, and creatine. In the artificial saliva, the creatine, glucose, and urea concentrations were less than 1, 50 and 100 μ M, respectively. The CoA signal is 4.5 times higher than those of creatine and glucose, and 3 times higher than that of urea (Fig. 2.6). Therefore, the results indicated that our biosensor could achieve high selectivity for real saliva sample measurements.

2.3.6 Recovery tests of spiked samples with carnitine in artificial saliva

Recovery test results for carnitine spiked in artificial saliva under an optimized carnitine biosensor are shown in Table 2.2. The calculated recovery values for artificial saliva samples were between 97.17 and 96.55 % with RSDs as low as 5.58 %. The results showed that our biosensor device is capable of highly sensitive and highly selective carnitine determination in saliva.

Table 2.2. Recovery of carnitine in artificial saliva samples (n=3)

Samples	Added (μM)	Detected (μM)	Recovery (%)	RSD (%)
I	10	9.72	97.17	5.58
II	20	19.31	96.55	8.61

Chapter 2.

2.4 Conclusion

The author developed a highly sensitive carnitine biosensor based on an enzyme-modified Au electrode combined with CSV measurement. The sensor can quantitatively detect carnitine by detecting CoA generated by the reaction of carnitine and acetyl-CoA generated by the enzymatic reaction of carnitine acetyltransferase. Although the CoA and acetyl-CoA could adsorb on the gold surface, the selective detection of CoA could be achieved thanks to their different desorption potentials and the optimization of the enzyme membrane composition, which realized the complete consumption of the acetyl-CoA diffused in the enzyme membrane. A detection limit of 0.025 μM and a linear detection range from 0.025 to 25 μM were obtained due to the accumulation of CoA on the Au electrode surface. The sensor also exhibited a good recovery of carnitine in artificial saliva sample. However, the Au bulk electrode is expensive and not suitable for mass-production, the development of film electrode for carnitine biosensor is required.

Chapter 2.

2.5 References

[1] J. Bremer, Carnitine--metabolism and functions, *Physiological Reviews*, 63(1983) 1420-80.

[2] C.J. Rebouche, Quantitative estimation of absorption and degradation of a carnitine supplement by human adults, *Metabolism*, 40(1991) 1305-10.

[3] R.-I. Stefan, R.G. Bokretsiou, J.F. van Staden, H.Y. Aboul-Enein, Simultaneous determination of L- and D-carnitine using a sequential injection analysis/amperometric biosensors system, *J Pharm Biomed Anal*, 33(2003) 323-8.

[4] M. Sugimoto, D.T. Wong, A. Hirayama, T. Soga, M. Tomita, Capillary electrophoresis mass spectrometry-based saliva metabolomics identified oral, breast and pancreatic cancer-specific profiles, *Metabolomics*, 6(2010) 78-95.

[5] P.E. Minkler, C.L. Hoppela, Determination of free carnitine and 'total' carnitine in human urine: derivatization with 4'-bromophenacyl trifluoromethanesulfonate and high performance liquid chromatography, *Clin Chim Acta*, 212(1992) 55-64.

[6] P.E. Minkler, C.L. Hoppel, Quantification of Free Carnitine, Individual Short- and Medium-Chain Acylcarnitines, and Total Carnitine in Plasma by High-Performance Liquid

Chapter 2.

Chromatography, Anal Biochem, 212(1993) 510-8.

[7] M. Kagawa, Y. Machida, H. Nishi, J. Haginaka, Direct Enantiomeric Purity Determination of Acetyl-L-carnitine by LC with a Ligand-Exchange Chiral Stationary Phase, Chromatographia, 62(2005) 239-44.

[8] K. Li, W. Li, Y. Huang, Determination of free L-carnitine in human seminal plasma by high performance liquid chromatography with pre-column ultraviolet derivatization and its clinical application in male infertility, Clin Chim Acta, 378(2007) 159-63.

[9] P.E. Minkler, S.T. Ingalls, C.L. Hoppel, Strategy for the Isolation, Derivatization, Chromatographic Separation, and Detection of Carnitine and Acylcarnitines, Anal Chem, 77(2005) 1448-57.

[10] K. Li, Q. Sun, Simultaneous Determination of Free and Total Carnitine in Human Serum by HPLC with UV Detection, J Chromatogr Sci, 48(2010) 371-4.

[11] K. Heinig, J. Henion, Determination of carnitine and acylcarnitines in biological samples by capillary electrophoresis-mass spectrometry, Journal of Chromatography B: Biomedical Sciences and Applications, 735(1999) 171-88.

Chapter 2.

[12] L. Sánchez-Hernández, M. Castro-Puyana, C. García-Ruiz, A.L. Crego, M.L. Marina, Determination of l- and d-carnitine in dietary food supplements using capillary electrophoresis–tandem mass spectrometry, *Food Chem*, 120(2010) 921-8.

[13] P. Andrieux, T. Kilinc, C. Perrin, E. Campos-Giménez, Simultaneous determination of free carnitine and total choline by liquid chromatography/mass spectrometry in infant formula and health-care products: Single-laboratory validation, *J AOAC Int*, 91(2008) 777-85.

[14] C.S. Ho, B.S.S. Cheng, C.W.K. Lam, Rapid Liquid Chromatography–Electrospray Tandem Mass Spectrometry Method for Serum Free and Total Carnitine, *Clin Chem*, 49(2003) 1189.

[15] L.M. Lewin, A. Peshin, B. Sklarz, A gas chromatographic assay for carnitine, *Anal Biochem*, 68(1975) 531-6.

[16] C. Costa, E. Struys, A. Bootsma, H. Brink, I. Almeida, M. Duran, et al., Quantitative analysis of plasma acylcarnitines using gas chromatography chemical ionization mass fragmentography, *J Lipid Res*, 38(1997) 173-82.

[17] G. Cederblad, S. Lindstedt, A method for the

Chapter 2.

determination of carnitine in the picomole range, Clin Chim Acta, 37(1972) 235-43.

[18] J.D. McGarry, D.W. Foster, An improved and simplified radioisotopic assay for the determination of free and esterified carnitine, J Lipid Res, 17(1976) 277-81.

[19] P.R. Borum, Carnitine: determination of total carnitine using a radioenzymatic assay, Journal of Nutritional Biochemistry, 1(1990) 111-4.

[20] K.-G. Seline, H. Johein, The determination of L-carnitine in several food samples, Food Chem, 105(2007) 793-804.

[21] L. Wan, R.W. Hubbard, Determination of free and total carnitine with a random-access chemistry analyzer, Clin Chem, 44(1998) 810.

[22] H. Kerspern, J.-L. Carré, Adaptation of free and total plasma carnitine determination on the Dimension® HM, X-Pand model (Dade Behring), Annales de biologie clinique, 66(2008) 207-11.

[23] M.S. Andrianova, E.V. Kuznetsov, V.P. Grudtsov, A.E. Kuznetsov, CMOS-compatible biosensor for L-carnitine detection, Biosens Bioelectron, 119(2018) 48-54.

[24] B. Zhang, Y. Zhang, W. Liang, B. Cui, J. Li, X. Yu, et al.,

Chapter 2.

Nanogold-penetrated poly(amidoamine) dendrimer for enzyme-free electrochemical immunoassay of cardiac biomarker using cathodic stripping voltammetric method, *Anal Chim Acta*, 904(2016) 51-7.

[25] W. Fan, X. Wang, X. Li, F. Xue, Determination of metallothionein in *Daphnia magna* by modified square wave cathodic stripping voltammetry, *Electrochem Commun*, 52(2015) 17-20.

[26] D. Wang, N. Gan, J. Zhou, P. Xiong, Y. Cao, T. Li, et al., Signal amplification for multianalyte electrochemical immunoassay with bidirectional stripping voltammetry using metal-enriched polymer nanolabels, *Sensors and Actuators B: Chemical*, 197(2014) 244-53.

[27] H. Matsuura, Y. Sato, O. Niwa, F. Mizutani, Electrochemical Enzyme Immunoassay of a Peptide Hormone at Picomolar Levels, *Anal Chem*, 77(2005) 4235-40.

[28] A. Yamada, Q. Feng, Q. Zhou, A. Hoskins, K.M. Lewis, B.D. Dunietz, Conductance of Junctions with Acetyl-Functionalized Thiols: A First-Principles-Based Analysis, *The Journal of Physical Chemistry C*, 121(2017) 10298-304.

[29] Z. Cao, D.M. Bassani, B. Bibal, Photoreduction of Thioether Gold(III) Complexes: Mechanistic Insight and

Chapter 2.

Homogeneous Catalysis, Chemistry, 24(2018) 18779-87.

[30] M. Weiwer, S. Olivero, E. Duñach, Product selectivity in the electroreduction of thioesters, Tetrahedron, 61(2005) 1709-14.

[31] D. Kato, T. Kamata, D. Kato, H. Yanagisawa, O. Niwa, Au Nanoparticle-Embedded Carbon Films for Electrochemical As³⁺ Detection with High Sensitivity and Stability, Anal Chem, 88(2016) 2944-51.

Chapter 3. the study of sputtered carbon film for gold nanoparticle-based biosensor

3.1 Introduction

In this chapter, the film electrode for detecting carnitine is studied to improve the performance of the carnitine biosensor. The film electrode is also important to apply for commercial biosensor which requires mass-production and low cost. The carbon film electrode was selected as a base electrode because it is stable and low noise. Then, the author modified the Au nanoparticles on the carbon film electrode to preconcentrate CoA generated by the enzymatic reaction of carnitine and acetyl-CoA. In the Introduction section, the author first introduced about carbon film electrode and then metal nanoparticles modified film electrodes.

3.1.1 Carbon film

Carbon films are widely employed in electrochemical analysis because they are mass-producible and can be fabricated with any shape and size.[1] Carbon films fabricated by the pyrolysis of organic (or polymeric) films can have a similar structure to that of glassy carbon,[2-5] which exhibits good electrochemical activity. However, the films are often porous and require the substrates to be used at very high temperature. In contrast, carbon films deposited by vacuum processes including direct current (DC)

Chapter 3.

magnetron sputtering,[6-8] radio frequency (RF) magnetron sputtering,[9, 10] electron cyclotron resonance (ECR) sputtering,[11, 12] electron beam evaporation,[13] and a filtered cathodic vacuum arc (FCVA) system,[14] produce flat but more amorphous structures similar to diamond-like carbon (DLC), which reduces electrochemical activity.

Ferrari et al. published a ternary phase diagram of amorphous carbons, which clearly shows the relationships between DLC structures and hydrogen, sp^2 and sp^3 carbons.[15] However, the diagram does not include high-order structural features such as degree of crystallinity, which is strongly related to electrochemical activity. Hirono et al. reported nanocarbon films formed by electron cyclotron resonance (ECR) sputtering.[11] The films contain a nano-graphene structure, which decreases with increasing sp^3 concentration. In contrast, ECR nanocarbon films with higher sp^3 concentrations have excellent electrochemical properties such as sufficient electrochemical activity, lower noise, and a wider potential window, as our group reported previously.[16, 17]

Kamata et al. subsequently reported similar carbon films prepared with unbalanced magnetron (UBM) sputtering.[18] The sp^2 and sp^3 ratios could be well controlled by the different subtracted bias voltage between the target and substrate. More recently, Diao et al. reported carbon films fabricated by ECR sputtering containing a larger graphene structure that was realized by using low-energy electron irradiating carbon atoms instead

Chapter 3.

of ion irradiation.[12, 19] The films have rougher surfaces than previously reported ECR nanocarbon films but exhibit better electrochemical activity. However, such equipment is not widely used and the cost is very high. In contrast, DC magnetron sputtering equipment has been commonly used to fabricate conducting films including carbon. Freire et al., Broitman et al., and Zeng et al. reported a DLC carbon film prepared with a DC magnetron sputtering method, and the amorphous carbon structure realized electrochemical stability, a lower capacitive current and a smaller surface area.[6-8] Although the sputtered carbon film electrodes show excellent electrochemical characteristics as described above, the film electrodes were required to have improved electrochemical activity for applying to carnitine biosensor because thiol compound cannot be preconcentrated onto the carbon electrode.

3.1.2 Metal nanoparticle modified carbon film electrode

Metal electrodes have excellent electrochemical activity, and are widely employed in the electrochemical analysis of heavy metals and thiol-containing biomolecules. Although the metal electrode has the characteristics mentioned above, its application in biosensing technology is limited. Because the biosensing technology required an electrode with not only high sensitivity but low background current, which is necessary to achieve a low detection limit. Metal nanoparticles (NPs) were widely

Chapter 3.

employed to modify on carbon film electrodes to improve the electrochemical activity of carbon film electrodes with maintaining low noise level. This is because limited surface area of the NPs suppresses the increase in background current since carbon surface shows low noise level. The sensitivity can be controlled by changing the amount of NPs modified on the carbon electrode. Various metal nanoparticles embedded (or modified) carbon film electrodes were employed for electroanalysis, including PtNPs embedded carbon film electrode applied in H₂O₂, glucose, acetylcholine and geosmin detection,[20, 21] PdNPs deposited carbon electrode applied in NO₂ detection,[22] NiNPs embedded carbon film electrodes applied in sugar detection,[23] CuNPs embedded carbon film electrode applied in glucose detection in alkaline solution,[24] AuNPs embedded and deposited carbon film electrodes applied in As³⁺, glucose and neuraminidase detection.[25-27] In the study of Wahyuni et al., the performance could be achieved as ng/mL level by using voltammetry measurement.[27] This result indicated that the AuNPs-based carbon film electrode could achieve a biosensor with trace level determination.

In this chapter, the author studied the structure and basic electrochemical properties of DC magnetron-sputtered carbon films prepared with different sputtering power, and then the carbon film surface was modified with AuNPs. The carnitine sensor was prepared by modifying with enzyme on the AuNPs modified carbon films.

Chapter 3.

The author expects the application of sputtering power to allow us to control such aspects of the film structure as sp^3 concentration and improve the ordering of the film thus realizing better electrochemical activity. The author characterized the surface structure of DC-sputtered carbon films using X-ray photoelectron spectroscopy (XPS) and transmission electron microscopy (TEM). The basic electrochemical properties were studied and compared with those of UBM-sputtered carbon films by measuring the cyclic voltammetry of several redox species with different electron-transfer properties. The effect of surface functional groups on the electrochemical properties was also studied by employing DC sputtered carbon films deposited under different conditions. This is because the content of surface functional groups can affect the electron transfer kinetics of organic biochemicals.[28] The deposition process of AuNPs on the DC carbon film was optimized, and the CV method was employed to evaluate the amount of deposited AuNPs. The performance of AuNPs-based biosensor was evaluated by CSV method. A low detection limit with the μM level was achieved by optimizing AuNPs deposition process parameters such as the deposition time and potentials, and the sp^3 concentrations of carbon film.

3.2 Experimental section

3.2.1 Reagents and materials

All of the chemicals employed in this study were of analytical grade and used as received without further purification. Hexaammineruthenium (III) chloride $[\text{Ru}(\text{NH}_3)_6]\text{Cl}_3$ and dopamine hydrochloride were purchased from Sigma-Aldrich (Tokyo, Japan). Potassium chloride (KCl), iron (II) chloride tetrahydrate ($\text{FeCl}_2 \cdot 4\text{H}_2\text{O}$), and potassium hexacyanoferrate (III) ($\text{K}_3[\text{Fe}(\text{CN})_6]$) were purchased from Wako Pure Chemical Industries (Tokyo, Japan). The glassy carbon electrode (GC) was purchased from BAS (Tokyo, Japan).

The gold standard solution (1000 ppm HAuCl_4) was purchased from Wako (Tokyo, Japan.), Bovine serum albumin (BSA) was obtained from Jackson ImmunoResearch Laboratories, Inc. (Pennsylvania, USA). Acetyl coenzyme A lithium salt (acetyl-CoA, enzymatic $\geq 93\%$) and carnitine acetyltransferase (40 unit/g) were purchased from Sigma-Aldrich (Tokyo, Japan). L-Carnitine was purchased from Fujifilm (Japan, Osaka). Glutaraldehyde (G.A.) 50 % (5 mM) water solution was purchased from KISHIDA CHEMICAL Co., Ltd. (Osaka, Japan). The artificial saliva used for the recovery experiment and selectivity study was purchased from Teijin (Tokyo, Japan), and composition is 14.44 μM NaCl, 16.11 KCl, 0.99

Chapter 3.

μM $\text{CaCl}_2 \cdot 2\text{H}_2\text{O}$, $0.55 \mu\text{M}$ MgCl_2 , and $1.96 \mu\text{M}$ K_2HPO_3 . Glucose, creatine, and urea were used as the interfering factors spiked in the artificial saliva for the selectivity studies, and glucose and creatine were purchased from Sigma-Aldrich (Tokyo, Japan) and urea was purchased Fujifilm (Japan, Osaka), respectively. The following buffer solutions were used: 0.1 M acetic acid buffer was used as the acetyl-CoA buffer. 0.1 M PB buffer (pH = 7.9) was used as the carnitine buffer, and the final pH of mixing buffers was 7.2.

3.2.2 Carbon film preparation

The carbon films were deposited on highly doped silicon (100) substrates with DC magnetron sputtering equipment at room temperature. The Ar gas pressure was 2.5×10^{-1} Pa. The substrate temperature was 200 °C, and the voltage and current of the target were 640 V and 0.68 A, respectively. The powers of target bias were 0, 12, 20, 30, and 35 W (namely, the target biases were 0, -130, -230, -300, and -350 V). The DC carbon film formation time was less than 5 mins.

3.2.3 Gold nanoparticles electrodeposition

The DC magnetron sputtered carbon film cut into a rectangular shape and the insulating tape with a 2-mm-diameter hole attached the film electrode in order to define the electrode surface area (0.0134 cm^2). The gold standard solution (1000 ppm HAuCl_4) was diluted 10-fold with 0.1 M H_2SO_4 for the further electrodeposition of AuNPs. The final solution of AuCl_4^- consists of 100 ppm AuCl_4^- , 0.1 M HCl, and 0.09 M H_2SO_4 . The prepared carbon film electrode immersed in the 100 ppm AuCl_4^- solute on, and applied the potentials of -0.15 V to the DC-magnetron sputtered carbon film for 240 s. After washing the electrode surface with pure water, the electrode was transferred into the 1.0 M H_2SO_4 solution for electrochemical cleaning by applied the potential scans from 0.1 V to 1.5 V for 6 cycles.

3.2.4 Carbon film characterization

The surface properties of the DC carbon films were characterized by X-ray photoelectron spectroscopy (XPS, ESCA Quantum 200, Ulvac-phi Co., Japan) using Al K α monochromatic X-rays (1486.6 eV) to determine the elemental composition and the quantity of chemical bonds in the carbon film electrode surfaces. The surface structure of the DC carbon films and UBM nano film were characterized by a high-resolution transmission electron microscopy (TEM, Tecnai Osiris, FEI Co., Japan) with a point-to-point resolution of 0.25 nm, and the acceleration voltage is 200 kV.

3.2.5 Electrochemical measurements of pure carbon films

Cyclic voltammograms (CVs) were obtained with an electrochemical analyzer (ALS model 720E BAS Co. Ltd., Tokyo, Japan) using a three-electrode system. DC carbon films, Ag/AgCl (RE-3 V BAS Co. Ltd., Tokyo Japan) and Pt wire were used as working, reference and counter electrodes, respectively. The electrolyte solutions in this study were deoxygenated by purging them with pure Ar gas for 20 mins before performing the electrochemical measurements.

3.2.6 Cathodic stripping voltammetry analysis

Square-wave cathodic stripping voltammetry (SWCSV) was performed with an enzyme-modified AuNPs-deposited carbon film electrode. Before the SWCSV measurement, the author prepared a 20 μL solution containing 500 nM carnitine and 500 nM acetyl-CoA and incubated it with the enzyme-modified electrode for 30 min. Then, the electrode was rinsed with deionized water. After rinsing, the electrode was immersed in a 0.5 M KOH solution for an SWCSV measurement. The measurements consisted of two steps: (i) 60s deposition at -0.8 V vs Ag/AgCl to preconcentrate CoA-SH. (ii) The working electrode was cathodic stripped from 0 to -1.8 V (vs. Ag/AgCl) by employing a frequency of 12.5 Hz, an amplitude of 20 mV, and a step potential of 4 mV.

3.3 Results and Discussion

3.3.1 Surface characterizations of DC sputter deposited carbon films

The author prepared DC magnetron sputtered carbon films under different conditions by changing the power of the target bias (0, 12, 20, 30, and 35 W). The carbon films were characterized by using XPS and TEM measurements. Figure 3.1 compares the C 1s TEM spectra of DC carbon films formed with different target powers (0, 12, and 30 W) and UBM carbon film formed at -20 V.

As shown in Fig. 3.S1(B), the C 1s XPS spectra were fitted into two peaks by using Shirley's method as the author reported previously.[16, 18] The peaks that appeared at 284.5, and 285.5 eV were assigned to sp^2 and sp^3 hybrids, respectively. And GC consists of sp^2 bonds, and approximately without sp^3 bonds, thus the sp^3/sp^3+sp^2 ratio of GC is 0 %.[29] The sp^3/sp^3+sp^2 ratio obtained from the C 1s XPS spectrum and the content of oxygen-containing functional groups obtained from the O 1s XPS spectrum are summarized in Table 3.1. The sp^3 ratio increased as the bias power increased from 0 bias to 12 W, and then the ratio gradually decreased as the bias was further increased from 12 to 35 W. The sp^3 content of DC carbon film is insufficient compared with that of UBM carbon film, suggesting that high-energy ion irradiation is beneficial as regards the

Chapter 3.

formation of sp^3 structures on the carbon surface during UBM sputtering. These results indicate that the sp^3 content could be successfully controlled by employing DC sputtering equipment, which is simpler and less expensive than ECR and UBM sputtering equipment.

The author also obtained the TEM images of the carbon films as shown in Fig. 3.1. The film prepared with a 0 W bias has an amorphous structure without any observable layered nanocrystalline graphite structures. With the bias increased to 12 W, layered structures can be observed. A further increase in bias up to 30 W increases the layered graphene structure as shown in Fig. 3.1 (C). In our previous report using UBM sputtering, the increase in the bias voltage from 0 to -75 V increased the size of the nanocrystalline structure and improved the electron transfer rate of $Fe(CN)_6^{4-/3-}$,¹⁸ which agrees well with the result the author obtained when the bias power increased from 0 bias to 12 W. Namely, the Ar⁺ ion irradiation energy can induce the rearrangement in the carbon film under sufficient sputtering power as one of the authors previously described. When the sputtering energy is insufficient, the ion irradiation is not enough to induce the rearrangement. In contrast, stronger ion irradiation by increasing bias power will greatly increase sp^3 concentration and suppress the formation of layered graphene structure. However, it is different from current results since the sp^2 ratio increased when the bias power increased to 30 W. Therefore, the sputtering condition must optimize and study the

Chapter 3.

mechanism with controlling the sp^3 ratio by DC magnetron sputtering.

Table 3.1 also shows the ratio of oxygen-containing functional groups and O/O+C ratios of DC carbon films prepared by different power of bias. The O/O+C ratio is varied from 5.21 to 4.67 at% and it tends to decrease as the current power increases, which might affect the electrochemical properties of redox species.

Table 3.1. Surface characterization data of DC carbon film electrodes

Power of bias	0 W	12 W	20 W	30 W	35 W
Surface group					
C=O (%)	23.6	26.1	23.3	32.0	33.1
ph-OH (%)	54.3	49.3	60.1	41.2	41.0
C-O (%)	20.5	20.9	15.1	25.3	24.6
$sp^3/(sp^3+sp^2)$	0.27	0.29	0.28	0.23	0.22
O/(C+O) (at%)	5.21	5.17	4.67	4.82	4.77

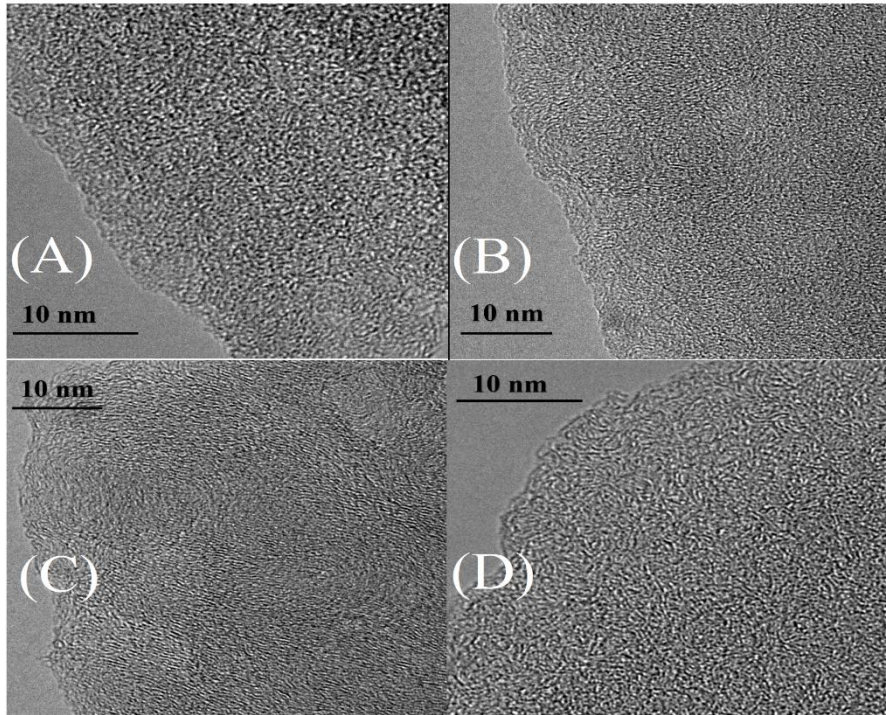


Figure 3.1. Surface TEM micrographs of carbon films: (A) DC 0 W; (B) DC 12 W; (C) DC 30 W; (D) UBM-20 V.

Chapter 3.

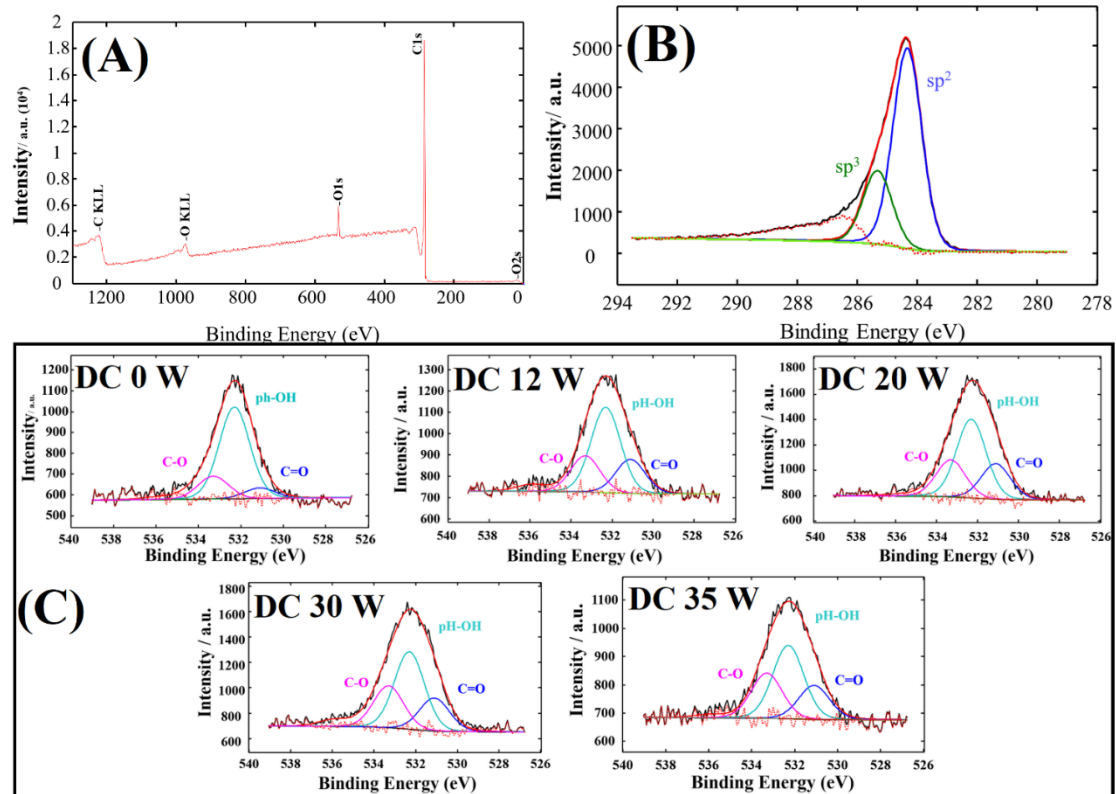


Figure 3.S1. XPS spectra of DC 0 W carbon films: (A) Total spectra. (B) C 1s spectra; (C) O 1s spectra of all DC- sputtered carbon films.

3.3.2 Potential windows of DC-sputtered carbon films

As previously reported with ECR and UBM sputtered carbon film electrodes, the author varied the sp^3 concentration and potential window by changing the bias between the target and the substrate. It is significant that excellent structures and properties of carbon films could be control using less expensive and commonly used DC sputtering equipment. Figure 3.2 shows voltammograms of GC and carbon films with different biases (12 and 30 W) in 0.05 M H_2SO_4 solution with a scan rate of 100 mV/s. The potential window is defined as the potential range between current limits that do not exceed $500 \mu A/cm^2$, as Swain et al. previously reported.[30] As shown in Fig. 3.2, the potential window of the film prepared with a bias is significantly extended compared with GC and 12 W film. Figure 3.3 shows the relationship between the sp^3/sp^3+sp^2 ratio of the GC and carbon films and their potential window. The potential window of a GC electrode is 2.70 V as shown in Fig. 3.2. The potential windows of carbon films increase from 2.90 to 3.44 V as the sp^3/sp^3+sp^2 ratio increases from 0.22 to 0.29, which agrees well with the results obtained with ECR and UBM sputtered carbon films, although the controllable range of the sp^3/sp^3+sp^2 ratio and the widths of the potential windows are limited.[16, 18]

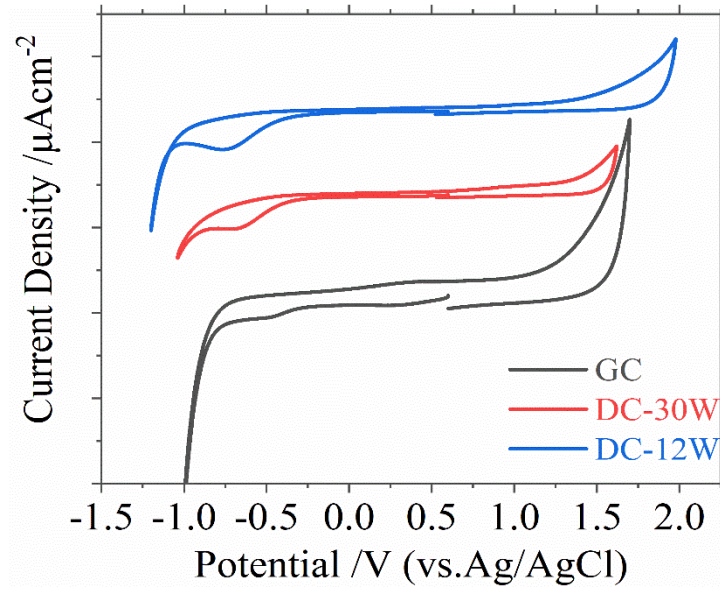


Figure 3.2. Voltammograms of DC carbon film electrodes in 0.05 M H₂SO₄ deoxygenated with Ar (scan rate, 100 mV/s).

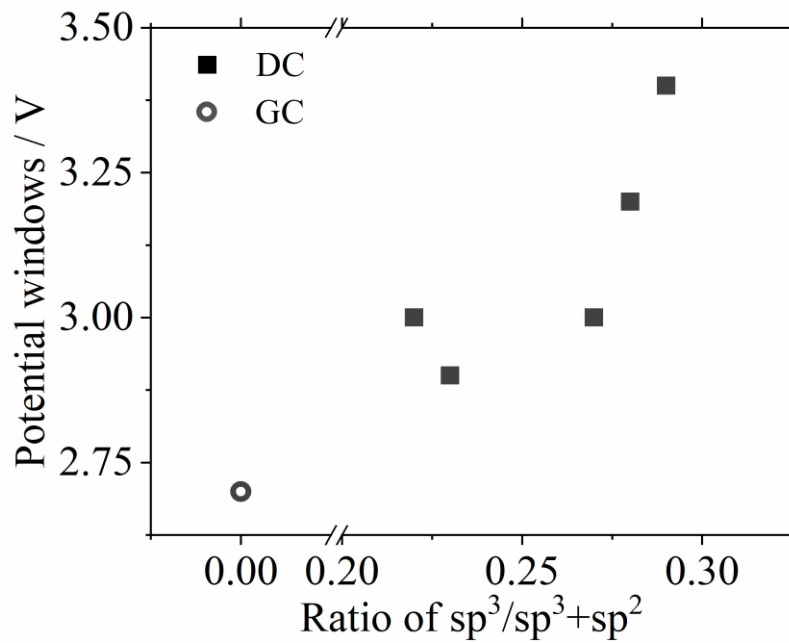


Figure 3.3. Comparison of potential window values at different DC-sputtered carbon films and GC electrode.

3.3.3 Basic electrochemical properties of DC carbon films

Since the redox behavior of electroactive species are varied by reflecting the carbon film structure, the author compared the responses of $\text{Ru}(\text{NH}_3)_6^{3+/2+}$, $\text{Fe}(\text{CN})_6^{4-/3-}$, $\text{Fe}^{2+/3+}$, and dopamine at DC-magnetron sputtered carbon film, UBM sputtered carbon film and commercially available GC electrodes as shown in Fig. 3.4. Figure 3.5 (A) and (B) show the relationships between the peak separations (ΔE) calculated from voltammograms and the $\text{sp}^3/\text{sp}^3+\text{sp}^2$ ratio. $\text{Ru}(\text{NH}_3)_6^{3+/2+}$ is known to be an outer-sphere redox system that is insensitive to surface functional groups. Therefore, the ΔE values of $\text{Ru}(\text{NH}_3)_6^{3+/2+}$ are similar at DC-magnetron sputtered carbon films with different sp^3 concentrations, UBM-sputtered carbon films and GC electrodes as shown in Fig. 3.4 (A) and Fig. 3.5 (A).

The voltammograms of 1 mM $\text{Fe}(\text{CN})_6^{4-/3-}$ at three carbon electrodes are shown in Fig. 3.4 (B). It has been reported that $\text{Fe}(\text{CN})_6^{4-/3-}$ is an inner-sphere redox system and sensitive to the edge-plane structure.[31] Therefore, GC shows the narrowest peak separation when compared with DC and UBM carbon films because GC has a much more ordered edge-plane graphene structure than DC magnetron and UBM carbon film electrodes. Kamata et al. reported that the nanocrystalline graphene

Chapter 3.

structures observed in a TEM image of UBM sputter deposited carbon film decreases with increasing sp^3 concentration.[18] With DC magnetron sputtered carbon film, the ΔE value of $Fe(CN)_6^{4-/3-}$ also increases with increasing sp^3 concentration as shown in Fig. 3.5 (B), which is similar but little inferior to the result for UBM carbon film. Unlike $Fe(CN)_6^{4-/3-}$, an $Fe^{2+/3+}$ redox system is sensitive to a group containing surface oxygen. In fact, a voltammogram of $Fe^{2+/3+}$ at a GC electrode reveals a smaller ΔE than those at UBM and DC magnetron sputtered carbon film electrodes. This is because the GC was well polished just before the measurement, and so surface oxidation could be minimized. The relationship between ΔE and $O_{Ph-OH}/(C+O)$ is shown in Fig. 3.5 (C), which clearly indicates that ΔE decreases with increasing surface O_{Ph-OH} concentration similar to the previous results obtained with UBM sputtered carbon film electrodes.[18] Figure 3.4 (D) compares voltammograms of DA at three carbon electrodes and Fig. 3.5 (D) shows the relationship between ΔE and $O_{Ph-OH}/(C+O)$ of DA. ΔE decreases with increasing $O_{Ph-OH}/(C+O)$. This result agrees well with previous work by McCreery et al. who reported that surface anionic sites improved the DA reaction rate by employing a GC electrode.[32] However, the correlation between ΔE and $O_{Ph-OH}/(C+O)$ is not as good as that observed with an $Fe^{2+/3+}$ redox system. Therefore, author also plotted the relationship between ΔE and sp^3/sp^3+sp^2 for DA as shown in Fig. 3.S2. ΔE increases as the sp^2 ratio decreases, suggesting that the amount of edge

Chapter 3.

plane also contributes to the redox reaction of DA. Since the redox properties of the above four redox systems agreed well with the results for UBM carbon films, carbon films formed by DC magnetron sputtering can be used for electrochemical measurement whose performance is not inferior to that of previously reported carbon films prepared with more expensive equipment.

Chapter 3.

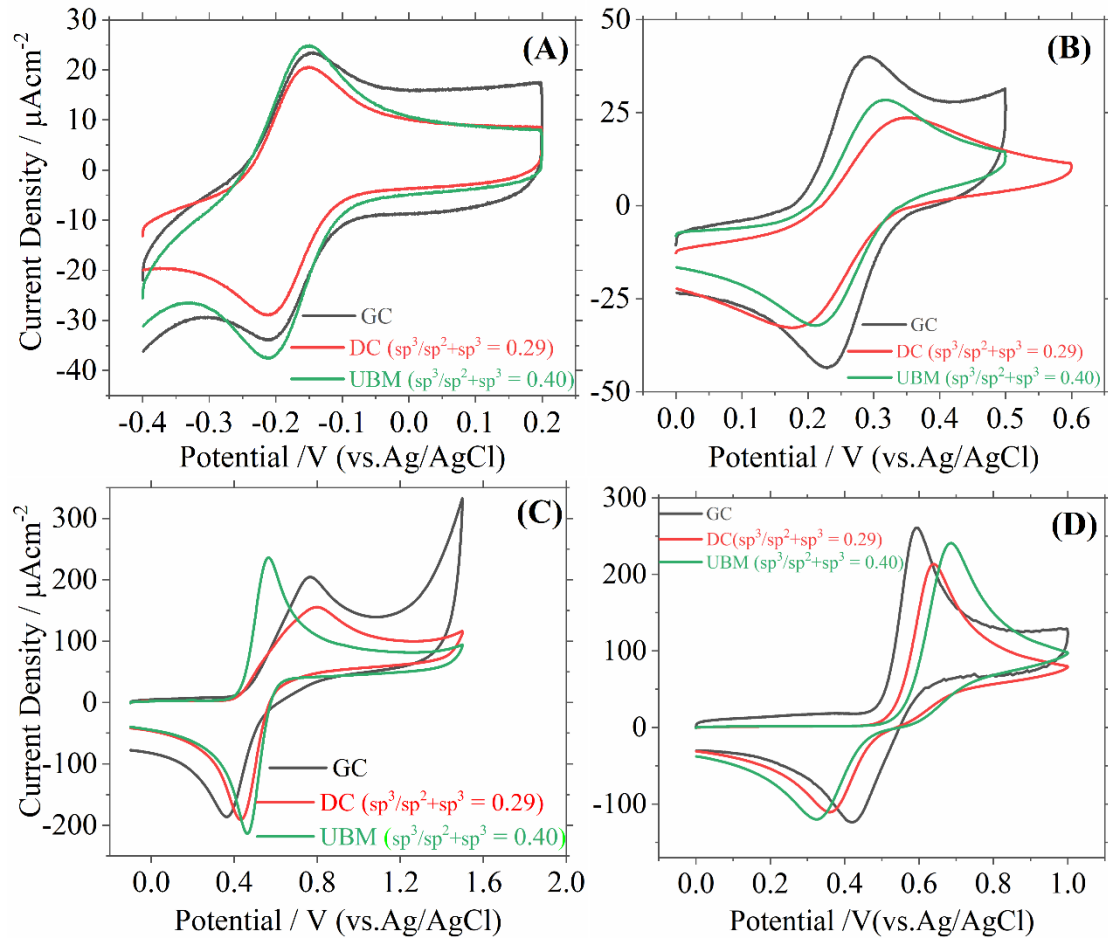


Figure 3.4. CVs of carbon film electrodes with: (A) 0.10 mM $\text{Ru}(\text{NH}_3)_6^{3+/2+}$ in 1.0 M KCl. (B) 0.10 mM $\text{Fe}(\text{CN})_6^{4-/3-}$ in 1.0 M KCl, (C) 1.0 mM $\text{Fe}^{2+/3+}$ in 0.1 M HClO_4 , and (D) 0.50 mM DA in 0.1 M HClO_4 , scan rate, 100 mV/s.

Chapter 3.

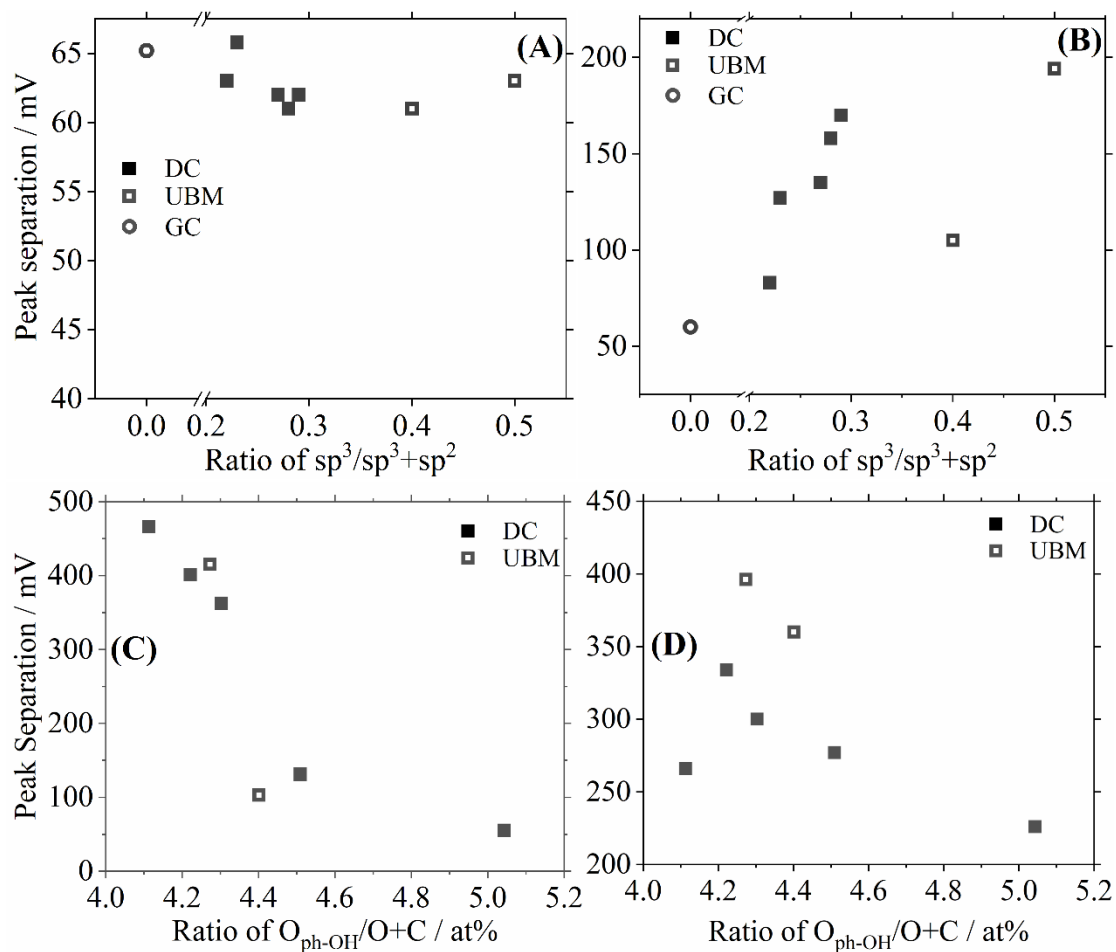


Figure 3.5. Comparison of peak separations at different electrodes obtained from (A) 0.10 mM $Ru(NH_3)_6^{3+/2+}$ in 1.0 M KCl. (B) 0.10 mM $Fe(CN)_6^{4-/3-}$ in 1.0 M KCl, (C) 1.0 mM $Fe^{2+/3+}$ in 0.1 M $HClO_4$, and (D) 0.50 mM DA in 0.1 M $HClO_4$, scan rate, 100 mV/s. (* The values for UBM carbon films were obtained from Kamata et al.¹⁸)

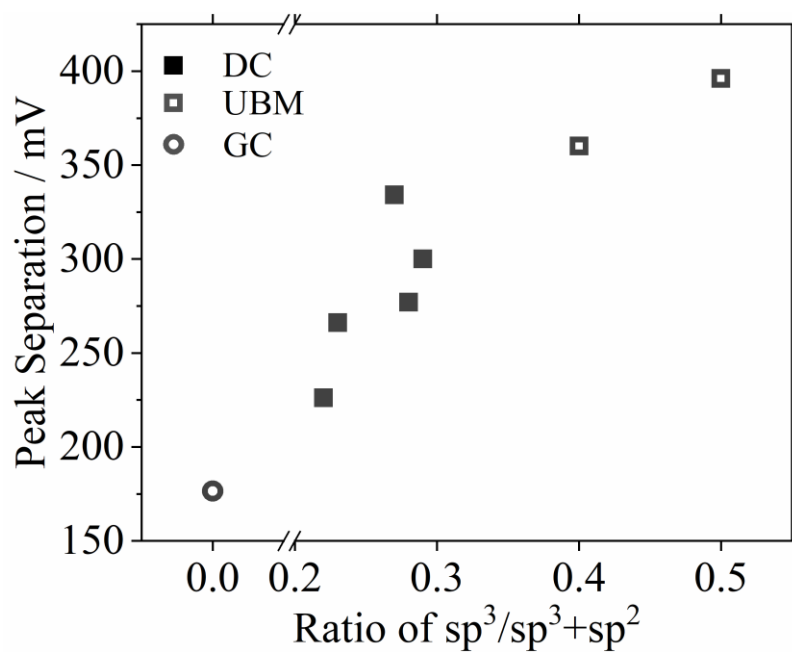


Figure 3.S2. Comparison of peak separations at different electrodes obtained from 0.50 mM DA in 0.1 M $HClO_4$, scan rate, 100 mV/s. (* The values for UBM carbon films were obtained from Kamata et al.¹⁸)

3.3.4 Optimization of AuNPs deposition parameters

To achieve a high selectivity of biosensors, the AuNPs deposition process was optimized as shown in Fig. 3.7. Before optimization studies, the author checked the deposition peak of AuNPs on a DC-magnetron sputtered carbon film. Figure 3.6 shows the electrochemical response of carbon film electrodes in 100 ppm AuCl_4^- solution. Only one peak can be observed at -0.02 V, which can be attributed to the deposition peak of AuNPs. Therefore, the author initially used a potential of -0.02 V as the deposition potential for the optimization study.

Figure 3.7 (a) shows the relationship between the deposition time and the CV curves with the deposition potential and the carbon film sp^3 concentration fixed at -0.02 V and 0.29%, respectively. When the deposition time increases, the peak of AuNPs also increases. A sufficient amount of AuNPs deposited on the carbon film electrode is necessary to achieve a sensitive carnitine biosensor. Therefore, author fixed the deposition time to 240 s for further experiments. Fig. 3.7(b) shows the variation in CV curves when the deposition potential is changed. The deposition potential ranges from 0 to -0.1 V with the fixed deposition time and sp^3 concentration of 240 s and 0.29 %, respectively. The deposition potential is sufficient, the magnitude of the AuNPs peak

Chapter 3.

increases significantly, suggesting that the sufficient potential improves the amount of deposited AuNPs. Therefore, author choose the -0.1 V deposition potential to realize a larger amount of deposited AuNPs on the carbon films.

Because the content of sp^3 in the carbon film will significantly affect the electrochemical performance (as described in 3.3.3), it will even further affect the deposition process of NPs. Therefore, the sp^3 (or sp^2) contents effect on AuNPs deposition process was studied as shown in Fig. 3.7 (c). The magnitude of AuNPs peak increases with increasing the sp^2 content. This result indicates that the AuNPs deposition rate was improved by increasing the sp^2 content, suggesting that the amount of edge plane also contributes to the AuNPs deposition process. Therefore, the more sp^2 content (which is sp^3 content = 0.22 %) of DC sputtered carbon film was selected as a base electrode in order to maintain sufficient amount of AuNPs deposition for realizing high sensitivity. The author also compared the CVs between Au bulk electrode and optimized AuNPs-based film electrode as shown in Fig. 3.8. The magnitude of the Au reduction peak of the Au bulk electrode is 8.5 times higher than that of the AuNPs-based film electrode. Therefore, it can estimate that the theoretical area of gold nanoparticles of the optimized AuNPs-based film electrode is 0.0024 cm^2 .

As summarized above, the author optimized AuNPs deposition

Chapter 3.

conditions as shown below. The deposition time is 240 s, the deposition potential is -0.1 V, and the sp^3 concentration in the DC carbon film is 0.22.

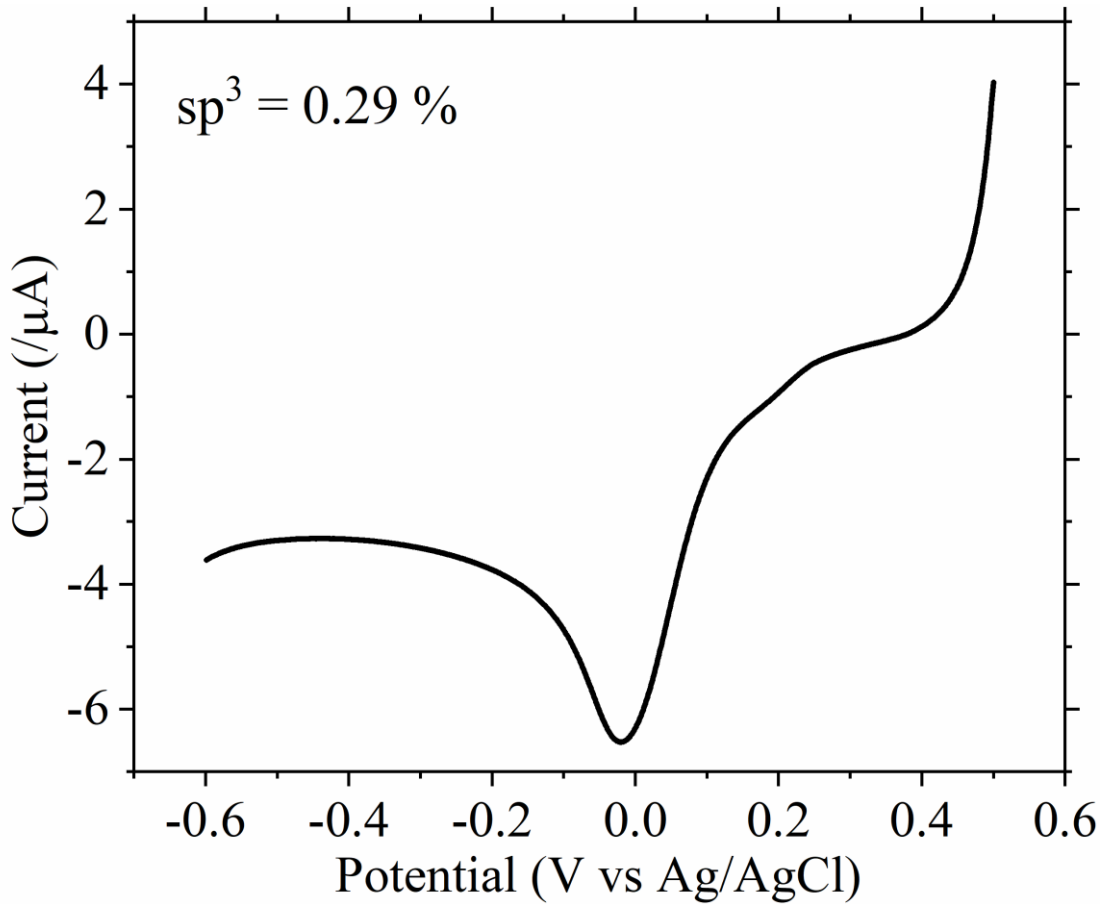


Figure 3.6. The deposition peak of AuNPs on the DC sputtered carbon film. (the sp^3 concentration of DC carbon film: 0.29; Electrolyte: 100 ppm $AuCl_4^-$ solution, scan rate: 0.05 V/s)

Chapter 3.

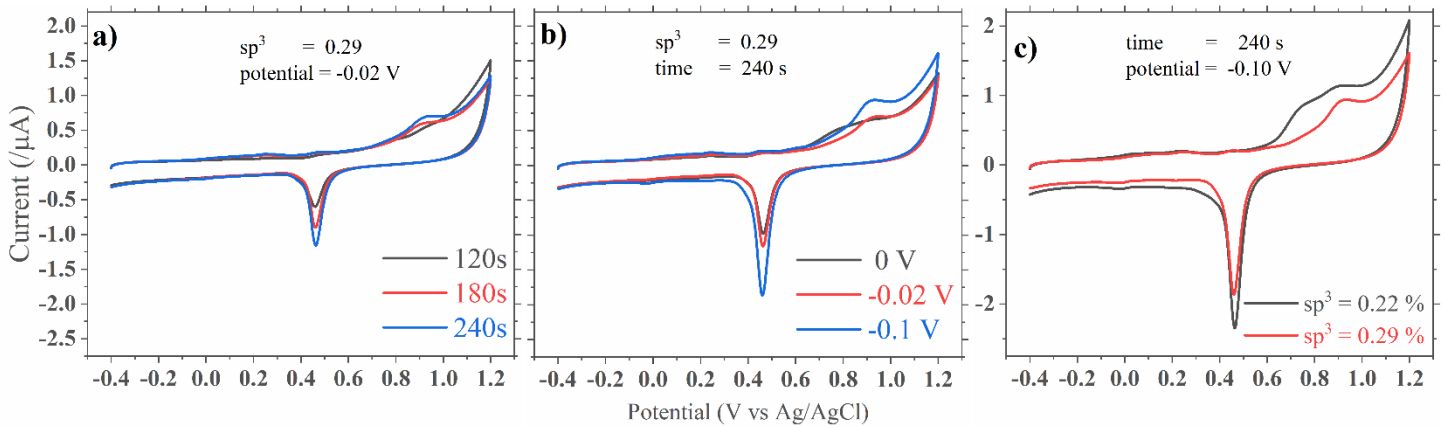


Figure 3.7. Optimization of the AuNPs deposition time, potential and sp^3 contents of carbon film base electrode. (a. Different deposition time; b. Different deposition potentials; c. Different sp^3 contents of base electrode; Electrolyte: 1 M H_2SO_4 ; scan rate: 0.1 V/s; scan range: from -0.4 to 1.2 V.)

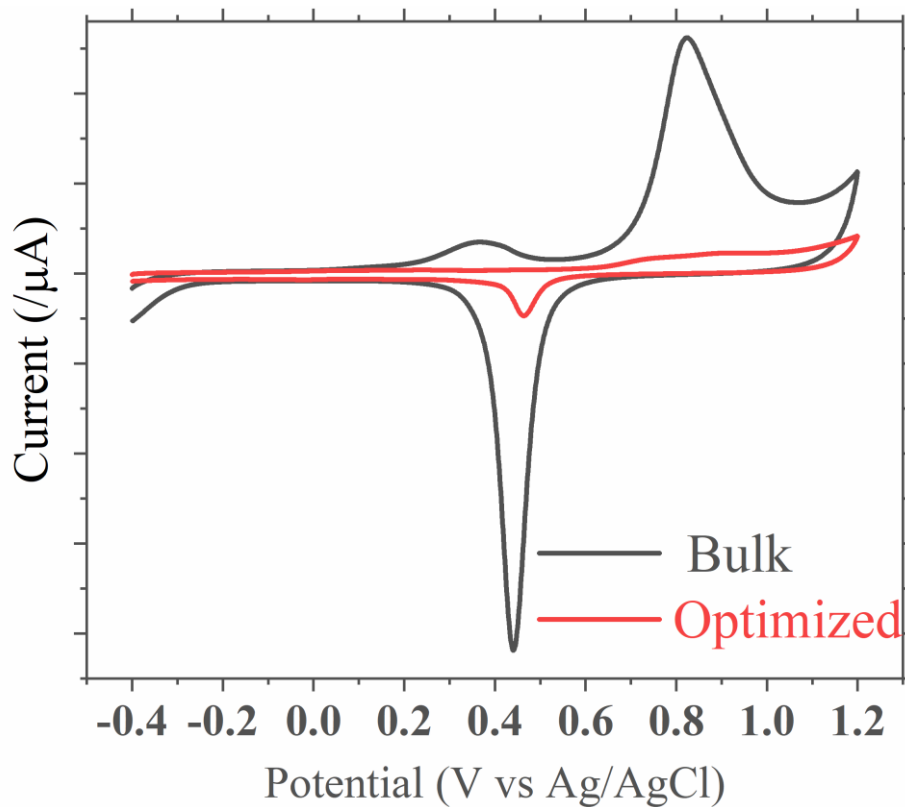


Figure 3.8. The CV curves of Au bulk electrode and optimized AuNPs-deposited carbon film electrode. (Electrolyte: 1 M H_2SO_4 ; scan rate: 0.1 V/s; scan range: from -0.4 to 1.2 V.)

3.3.5 Electrochemical behavior of CoA and acetyl-CoA on a AuNPs modified carbon film electrodes

Since the deposition process of AuNPs has been optimized, the performance of the AuNPs-based carnitine sensor should be studied subsequently. Before constructing biosensor by modifying enzyme, the electrochemical behaviors of CoA and acetyl-CoA on the AuNPs modified carbon film electrode should be studied because the behavior of such molecules on AuNPs might be different from that at Au bulk electrode.

Fig. 3.9 shows the CSV curves of CoA with different concentrations ranging from 0 to 1000 μM . The CoA reduction peaks were negatively shifted to -1.6 V compared to -1.2 V observed using the gold bulk electrode. This result indicates that AuNPs-based carbon film electrodes exhibit a more substantial binding capacity than Au bulk electrodes. It might be caused by the interactions between the CoA and the AuNPs or the AuNPs between DC-sputtered carbon films. Furthermore, the reduction peak current density of CoA is significantly improved by using AuNPs-based electrode compared with that of the Au bulk electrode. A Similar result have been reported by Kato et al.[33]

3.3.6 Electrochemical behavior of carnitine biosensor

Based on the results reported in 3.3.4, the author fabricated enzyme modified AuNPs modified carbon film electrodes. The enzyme membrane composition is the same as the author described in 2.3.2.

The performance of the AuNPs-based carnitine biosensor was shown in Figure 3.10. With the enzyme membrane modified on the AuNPs based electrode, only one peak was clearly observed at -1.6 V, and it belongs to CoA. Moreover, the reduction peak of CoA increases with increasing carnitine and acetyl CoA concentrations. This result shows that the enzymatic reaction has successfully occurred on the AuNPs modified carbon film electrode, and the carnitine enzymatic reaction product CoA could be selectively detected.

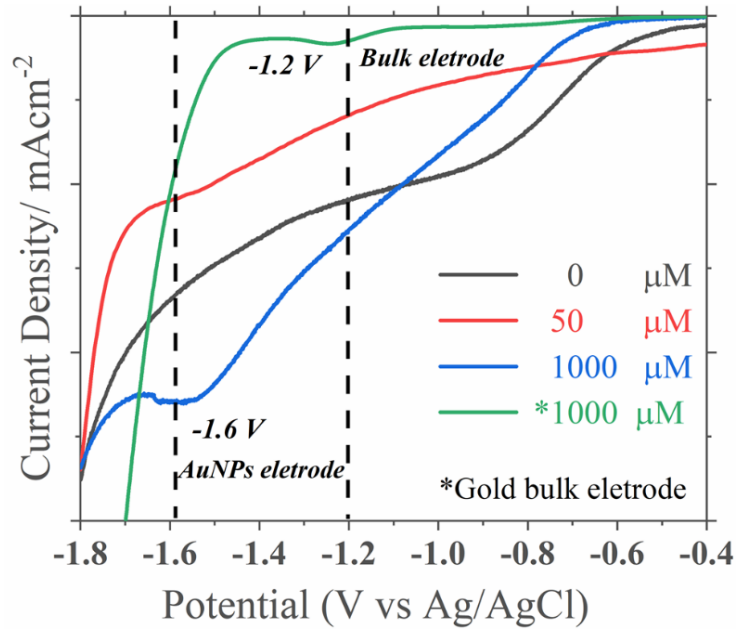


Figure 3.9. CSV curves of different CoA concentrations with an AuNPs-modified carbon film electrode. (Electrolyte: 0.5M KOH solution, scan rate: 0.05V/s)

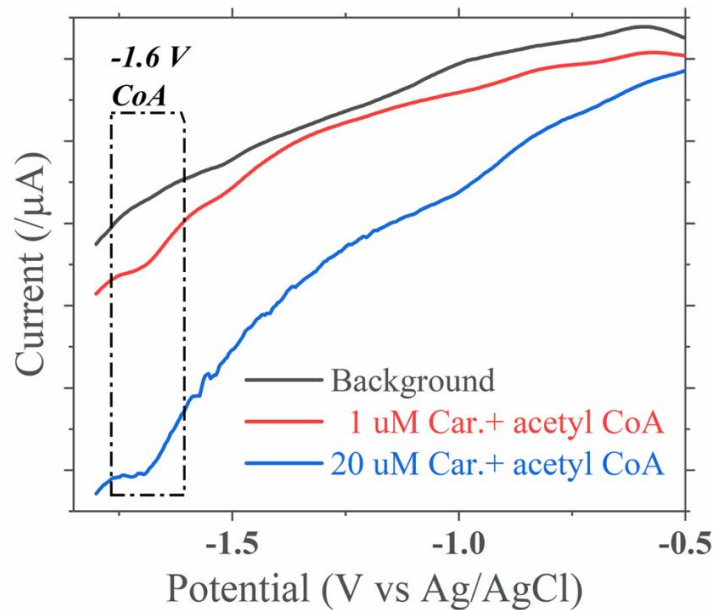


Figure 3.10. CSV curves of different carnitine and acetyl-CoA concentrations with an enzyme and AuNPs modified carbon film electrode. (Sample solution: PB buffer (pH =7.9) containing 500nM carnitine, and cofactor(acetyl-CoA) solution: acetic acid buffer (pH= 5.0) 500nM acetyl-CoA; the final pH of buffer solution: 7.2) Electrochemical desorption: in pH 13.5, Scan rate: 50mV/s.)

3.3.7 Carnitine calibration curves of AuNPs-based biosensor

The relationship between the CoA reduction current and the carnitine concentration was shown in Fig. 3.11. The author obtained the linear range for carnitine from 0.25 μM to 20 μM where the regression equation is $Y(-10^{-6}\text{VA}^{-1}) = 0.355 * X + 4.364$ ($R^2 = 0.9488$). When the carnitine concentration exceeds 20 μM , the peak current was almost saturated. This is because the amount of deposited AuNPs on the carbon film is insufficient, leading to the saturation of produced CoA adsorption.

The calculated detection limit was 0.25 μM ($S/N = 3$). Although the result is not as good as the bulk electrode, it is an acceptable result for the clinical trials. This might occur because of the interaction between the AuNPs and carbon film. Therefore, the variation of interaction by changing the base electrode including termination with other atoms such as nitrogen and fluorine will improve the performance of the biosensor.

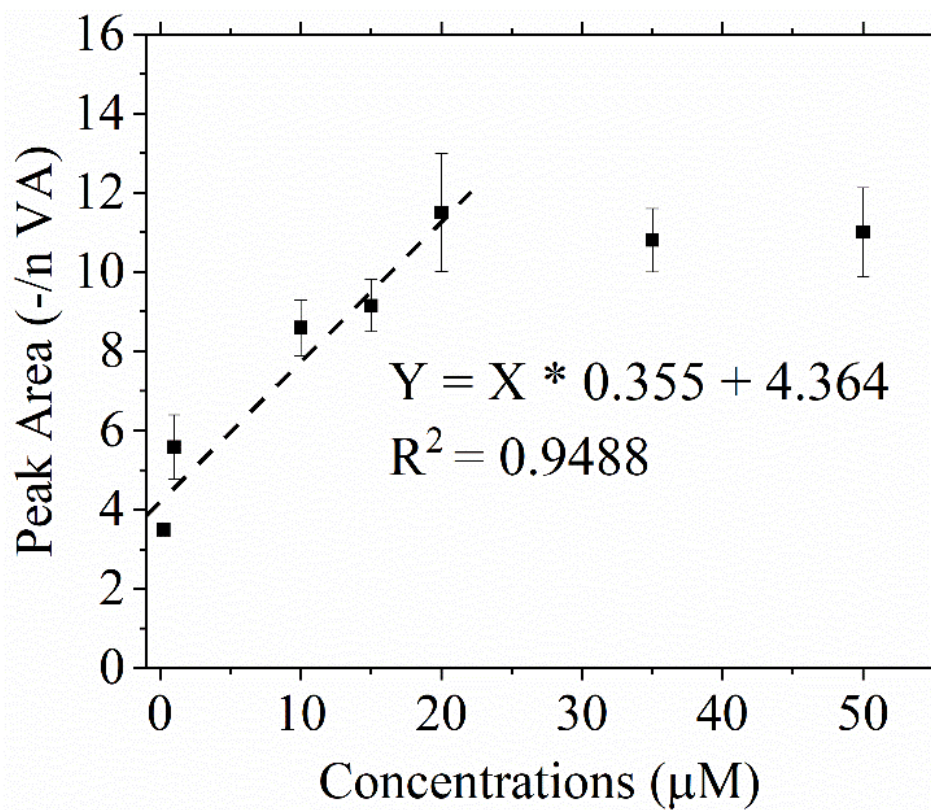


Figure 3.11. Relationship between CoA reduction current and carnitine concentration by using carnitine biosensor.

3.3.8 Selectivity study of carnitine biosensor

To conduct the selective study, three interfering factors were spiked in artificial saliva, namely glucose, urea, and creatine. In the artificial saliva, the creatine, glucose, and urea concentrations were less than 1, 50 and 100 μ M, respectively. Furthermore, the author also spiked 0.4 % BSA into the artificial saliva samples to simulate the protein content in real human saliva samples. Figure 3.12 shows the CoA signal is 2 times higher than those urea, creatine, and glucose. Therefore, the results indicated that this AuNPs-based carnitine biosensor could achieve acceptable selectivity for real saliva sample measurements.

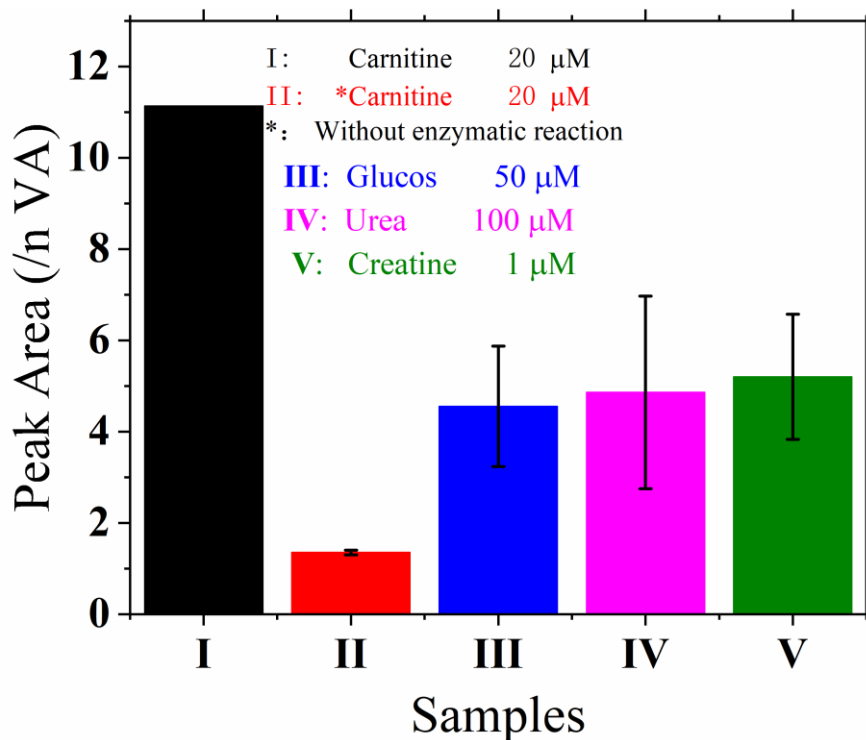


Figure 3.12. Selectivity studies with possible interferents with carnitine biosensor.

3.3.9 Recovery in artificial saliva with carnitine biosensor based on AuNPs modified carbon film

The recovery test results for carnitine spiked in artificial saliva by using a AuNPs-based carnitine biosensor were shown in Table 3.2. The artificial saliva also spiked 0.4% BSA solution in order to simulate the protein content in real human saliva samples. The calculated recovery values for artificial saliva samples were between 92.05 and 95.30 % with RSDs as low as 4.1 %. This result showed that the AuNPs-based carnitine biosensor the author developed has high selectivity and sensitivity carnitine determination even in real saliva samples.

Table 3.2. Recovery of carnitine in artificial saliva samples (n = 3)

samples	Added (μM)	Detected (μM)	Recovery (%)	RSD (%)
I	10	9.53	95.3%	8.5
II	20	18.41	92.05	4.1

3.4 Conclusion

This chapter studied to fabricate a disposable type carnitine biosensor. Therefore, the author first developed base carbon film electrode formed by DC-magnetron sputtering. Then, the author deposited AuNPs on the optimized carbon film and modified enzyme to realize carnitine biosensor.

About carbon film, the author studied the structure, and electrochemical properties of DC-magnetron sputtered carbon film electrodes prepared with different bias powers and compared the results with those obtained for previously studied UBM sputtered carbon film and GC electrodes. The sp^3 concentration of DC carbon films could be controlled (from 0.22 to 0.29) by different sputtering powers, and the potential windows increase with increasing sp^3 concentration. The redox reaction of four redox species agreed well with our group previous results obtained with UBM sputtered carbon films. This result indicates a carbon film electrode with good electrochemical properties even comparable with a UBM nanocarbon film electrode can be fabricate using DC-magnetron sputtering equipment.

After obtaining optimized carbon film, AuNPs was electrochemically deposited on the DC carbon film to apply for base electrode of a carnitine biosensor. The deposition process of AuNPs on the DC carbon film was optimized, and the CV method was employed to evaluate the amount of

Chapter 3.

deposited AuNPs. The amount of the AuNPs was improved when the deposition time and potential are sufficient. Moreover, the sp^2 contents could also improve the AuNPs deposition rate, indicating that graphite structure with more edge plane accelerates the electrodeposition of Au. The electrochemical reduction potential of CoA on the AuNPs-deposited carbon film electrode is more negative compared with a bulk electrode. This might be due to the interactions between CoA and AuNPs, or between AuNPs and DC-sputtered carbon films. As a result, an acceptable performance with a linear detection ranges from 0.25 μM to 20 μM and a LOD of 0.25 μM were achieved for carnitine determination in artificial saliva sample.

Although the AuNPs-based biosensor's detection limit currently cannot be superior to that of the Au bulk biosensor, the optimization of carbon film such as nitrogen doping and size and structure of AuNPs will improve the sensor performance.

3.5 References

[1] O. Niwa, Electroanalytical Chemistry with Carbon Film Electrodes and Micro and Nano-Structured Carbon Film-Based Electrodes, Bull Chem Soc Jpn, 78(2005) 555-71.

[2] M.L. Kaplan, P.H. Schmidt, C.H. Chen, W.M. Walsh, Carbon films with relatively high conductivity, Appl Phys Lett, 36(1980) 867-9.

[3] A. Rojo, A. Rosenstratten, D. Anjo, Characterization of a conductive carbon film electrode for voltammetry, Anal Chem, 58(1986) 2988-91.

[4] S. Ranganathan, R.L. McCreery, Electroanalytical Performance of Carbon Films with Near-Atomic Flatness, Anal Chem, 73(2001) 893-900.

[5] M. Morita, K. Hayashi, T. Horiuchi, S. Shibano, K. Yamamoto, K. Aoki, Enhancement of Redox Cycling Currents at Interdigitated Electrodes with Elevated Fingers, J Electrochem Soc, 161(2014) H178-H82.

[6] L.G. Jacobsohn, F.L. Freire, Influence of the plasma pressure on the microstructure and on the optical and mechanical properties of amorphous carbon films deposited by direct current magnetron sputtering, Journal of Vacuum

Chapter 3.

Science & Technology A: Vacuum, Surfaces, and Films, 17(1999) 2841-9.

[7] N. Hellgren, M.P. Johansson, B. Hjörvarsson, E. Broitman, M. Östblom, B. Liedberg, et al., Growth, structure, and mechanical properties of CN_xHy films deposited by dc magnetron sputtering in N₂/Ar/H₂ discharges, Journal of Vacuum Science & Technology A, 18(2000) 2349-58.

[8] A. Zeng, E. Liu, I.F. Annergren, S.N. Tan, S. Zhang, P. Hing, et al., EIS capacitance diagnosis of nanoporosity effect on the corrosion protection of DLC films, Diamond Relat Mater, 11(2002) 160-8.

[9] R. Schnupp, R. Kühnhold, G. Temmel, E. Burte, H. Ryssel, Thin carbon films as electrodes for bioelectronic applications, Biosens Bioelectron, 13(1998) 889-94.

[10] S. Logothetidis, G. Stergioudis, Studies of density and surface roughness of ultrathin amorphous carbon films with regards to thickness with x-ray reflectometry and spectroscopic ellipsometry, Appl Phys Lett, 71(1997) 2463-5.

[11] S. Hirono, S. Umemura, M. Tomita, R. Kaneko, Super-hard conductive carbon nano-crystallite films, Molecular Crystals and Liquid Crystals, 386(2002) 179-82.

[12] L. Huang, Y. Cao, D. Diao, Nanosized graphene sheets

Chapter 3.

induced high electrochemical activity in pure carbon film, *Electrochim Acta*, 262(2018) 173-81.

[13] J.J. Blackstock, A.A. Rostami, A.M. Nowak, R.L. McCreery, M.R. Freeman, M.T. McDermott, Ultraflat Carbon Film Electrodes Prepared by Electron Beam Evaporation, *Anal Chem*, 76(2004) 2544-52.

[14] H. Yu, P. Li, J. Robertson, Fabrication and bio-functionalization of tetrahedral amorphous carbon thin films for bio sensor applications, *Diamond Relat Mater*, 20(2011) 1020-5.

[15] A.C. Ferrari, J. Robertson, Resonant Raman spectroscopy of disordered, amorphous, and diamondlike carbon, *Physical Review B*, 64(2001).

[16] J. Jia, D. Kato, R. Kurita, Y. Sato, K. Maruyama, K. Suzuki, et al., Structure and Electrochemical Properties of Carbon Films Prepared by a Electron Cyclotron Resonance Sputtering Method, *Anal Chem*, 79(2007) 98-105.

[17] O. Niwa, J. Jia, Y. Sato, D. Kato, R. Kurita, K. Maruyama, et al., Electrochemical Performance of Angstrom Level Flat Sputtered Carbon Film Consisting of sp² and sp³ Mixed Bonds, *J Am Chem Soc*, 128(2006) 7144-5.

[18] T. Kamata, D. Kato, H. Ida, O. Niwa, Structure and

Chapter 3.

electrochemical characterization of carbon films formed by unbalanced magnetron (UBM) sputtering method, *Diamond Relat Mater*, 49(2014) 25-32.

[19] L. Huang, Y. Cao, D. Diao, Electrochemical activation of graphene sheets embedded carbon films for high sensitivity simultaneous determination of hydroquinone, catechol and resorcinol, *Sensors and Actuators B: Chemical*, 305(2020) 127495.

[20] T. You, O. Niwa, M. Tomita, S. Hirono, Characterization of Platinum Nanoparticle-Embedded Carbon Film Electrode and Its Detection of Hydrogen Peroxide, *Anal Chem*, 75(2003) 2080-5.

[21] T. Kamata, M. Sumimoto, S. Shiba, R. Kurita, O. Niwa, D. Kato, Increased electrode activity during geosmin oxidation provided by Pt nanoparticle-embedded nanocarbon film, *Nanoscale*, 11(2019) 8845-54.

[22] X.-H. Pham, C.A. Li, K.N. Han, B.-C. Huynh-Nguyen, T.-H. Le, E. Ko, et al., Electrochemical detection of nitrite using urchin-like palladium nanostructures on carbon nanotube thin film electrodes, *Sensors and Actuators B: Chemical*, 193(2014) 815-22.

[23] T. You, O. Niwa, Z. Chen, K. Hayashi, M. Tomita, S.

Chapter 3.

Hirono, An Amperometric Detector Formed of Highly Dispersed Ni Nanoparticles Embedded in a Graphite-like Carbon Film Electrode for Sugar Determination, *Anal Chem*, 75(2003) 5191-6.

[24] T. You, O. Niwa, M. Tomita, H. Ando, M. Suzuki, S. Hirono, Characterization and electrochemical properties of highly dispersed copper oxide/hydroxide nanoparticles in graphite-like carbon films prepared by RF sputtering method, *Electrochem Commun*, 4(2002) 468-71.

[25] Y. Song, G.M. Swain, Development of a Method for Total Inorganic Arsenic Analysis Using Anodic Stripping Voltammetry and a Au-Coated, Diamond Thin-Film Electrode, *Anal Chem*, 79(2007) 2412-20.

[26] A. Liu, E. Liu, G. Yang, N.W. Khun, W. Ma, Non-enzymatic glucose detection using nitrogen-doped diamond-like carbon electrodes modified with gold nanoclusters, *Pure Appl Chem*, 82(2010) 2217-29.

[27] W.T. Wahyuni, T.A. Ivandini, E. Saepudin, Y. Einaga, Development of neuraminidase detection using gold nanoparticles boron-doped diamond electrodes, *Anal Biochem*, 497(2016) 68-75.

[28] N. Sekioka, D. Kato, A. Ueda, T. Kamata, R. Kurita, S.

Chapter 3.

Umemura, et al., Controllable electrode activities of nano-carbon films while maintaining surface flatness by electrochemical pretreatment, *Carbon*, 46(2008) 1918-26.

[29] J. Díaz, G. Paolicelli, F. Salvador, F. Comin, Separation of the sp^3 and sp^2 components in the C1s photoemission spectra of amorphous carbon films, *Physical review B, Condensed matter*, 54(1996) 8064-9.

[30] Q. Chen, G.M. Swain, Structural Characterization, Electrochemical Reactivity, and Response Stability of Hydrogenated Glassy Carbon Electrodes, *Langmuir*, 14(1998) 7017-26.

[31] P. Chen, R.L. McCreery, Control of Electron Transfer Kinetics at Glassy Carbon Electrodes by Specific Surface Modification, *Anal Chem*, 68(1996) 3958-65.

[32] S.H. DuVall, R.L. McCreery, Self-catalysis by Catechols and Quinones during Heterogeneous Electron Transfer at Carbon Electrodes, *J Am Chem Soc*, 122(2000) 6759-64.

[33] D. Kato, T. Kamata, D. Kato, H. Yanagisawa, O. Niwa, Au Nanoparticle-Embedded Carbon Films for Electrochemical As^{3+} Detection with High Sensitivity and Stability, *Anal Chem*, 88(2016) 2944-51.

Chapter 4. Conclusions

In this thesis, we developed the highly sensitive carnitine biosensors based on enzyme modified Au bulk electrode and AuNPs-deposited DC sputtered carbon film electrode using cathodic stripping voltammetry measurement. The detection limit, selectivity, and recovery experiment of carnitine biosensors were studied after optimizing enzyme modification and CSV measurement conditions.

In chapter 2, the electrochemical behavior of CoA and acetyl-CoA, optimization of the enzyme membrane contents, and the position of the enzyme membrane were studied in order to develop the carnitine biosensor on the Au bulk electrode. Although both CoA and acetyl-CoA can be detected by the CSV method, CoA could be selectively detected since the potentials of reduction peaks were different. The performance of the sensor was optimized by adjusting BSA, GA and enzyme concentration.

The performance of Carnitine detection is also affected by the diffusion distance of CoA produced by the enzymatic reaction, which was studied by changing the position of modified enzyme membrane including just above the electrode and surrounded electrode. The linear range 0.25 to 20 μM and detection limit of 0.25 μM was obtained with sufficient selectivity against glucose, urine, and creatine. The detection of carnitine

in artificial saliva was successfully performed with good recovery.

In chapter 3, the carbon film fabricated by DC-magnetron sputtering method was employed to realize a deposable carnitine sensor. Since CoA generated by the enzymatic reaction of carnitine cannot be preconcentrated on the pure carbon film, the sensor was prepared after modifying AuNPs by electrochemical deposition.

The carbon films prepared with different bias powers and their structures were compared with those obtained for previously studied UBM sputtered carbon film and GC electrodes. Through the results of electrochemical measurements with four redox substances, XPS analysis, and TEM images, the results obtained from DC sputtered carbon film are similar to those of UBM nanocarbon films. The deposition process of AuNPs on the DC carbon film was optimized, and the CV method was employed to evaluate the amount of deposited AuNPs. The amount of the AuNPs was improved when the deposition time and potential are sufficient. Moreover, the sp^2 contents could also improve the AuNPs deposition rate, graphite structure with more edge plane accelerates the electrodeposition of Au. The electrochemical reduction potential of CoA on the AuNPs-deposited carbon film electrode is more negative compared with a bulk electrode. This might occur because of the interactions between the CoA and the AuNPs, or the AuNPs between DC-sputtered carbon films. Although the AuNPs-based biosensor's detection limit currently cannot be

improved compared with that of the Au bulk biosensor, the optimization of carbon film such as nitrogen doping and AuNPs such as size and structure will improve the performance.

The author believes that the carnitine biosensors developed and the research on DC magnetron sputtering carbon film in this thesis could be promising for the development of biosensors and non-invasive detection.

List of Achievements

Publications

Publications related to this thesis

1. **Zixin Zhang**, Osamu Niwa, Shunsuke Shiba, Shizuo Tokito, Kuniaki Nagamine, Shigeo Ishikawa, Masahiro Sugimoto. Electrochemical enzyme biosensor for carnitine detection based on cathodic stripping voltammetry. *Sensors and Actuators B: Chemical*, 321, (2020), 128473.
2. **Zixin ZHANG**, Saki OHTA, Tatsuhiko YAJIMA, Yoichi HIRUKAWA, Osamu NIWA. The basic electrochemical properties and structure of direct current magnetron sputtered carbon films. *Electrochemistry*. doi.org/10.5796/electrochemistry.20-00142.

Other publication

3. Osamu Niwa, Saki Ohta, Shota Takahashi, **Zixin Zhang**, Tomoyuki Kamata, Dai Kato, and Shunsuke Shiba. Hybrid carbon film electrodes for electroanalysis. *Analytical Sciences*. 10.2116/analsci.20SAR15.

International conference

Poster presentation

1. A study on electrochemical detection of carnitine using high sensitivity enzyme-based biosensor. **Zixin Zhang**, Osamu Niwa, Shunsuke Shiba, Kuniaki Nagamine, Shizuo Tokito, Shigeo Ishikawa, Masahiro Sugimoto. The Seventeenth International Symposium on Electroanalytical Chemistry & The Third International Meeting on Electrogenerated Chemiluminescence (17th ISEAC & 3rd ECL) August 22-25, 2019, Changchun, China.

List of Achievements

Award

The top-twenty excellent poster presentations in the 17th ISEAC & 3rd ECL.

Acknowledgement

I would like to express special appreciation and thanks to my advisor Professor Dr. Osamu Niwa. He has been a tremendous mentor for me. I would like to thank him for encouraging research and allowing me to grow as a research scientist. His advice on both research as well as on my career has been invaluable. I would also like to thank committee members, professor Tatsuhiko Yajima, professor Matsuo Tanaka, professor Yasushi Hasebe, and professor Susumu Saito for serving as my committee members' hardship. I also want to thank them for letting my defense be an enjoyable moment and for your thoughtful comments and suggestions.

I would especially like to thank the member of the Niwa group at Saitama Institute of Technology. All of them have been support my Ph.D study in 3 years. I would like to thank Professor Masahiro Sugimoto (Tokyo Medical University), and Professor Shizuo Tokito, Associate Professor Kuniaki Nagamine (ROEL, Yamagata University), and Assistant professors Shigeo Ishikawa (Yamagata University), and Shunsuke Shiba (Ehime University) for their help in Chapter 2. In addition, I would also like to thank Dr. Kan Hong for his support of academic and encouragement. I would also like to thank Drs. Tomoyuki Kamata, Dai Kato and Mr. Noriyuki Saitou working at AIST for their help in sample analysis.

Acknowledgements

To my old friend Mr. Xiaodong Su, I would like to express my thanks to him, because he is the man who courage me to go abroad, and company with me in his free time. A special thanks to my family. Words cannot express my gratitude to my grandmother, father, and mother for their psychological and financial support. Finally, I want to thank my grandfather for giving me the courage to overcome difficulties even in darkness mid-night. Wish that you could know I did it. Wish that I could tell you by myself. Wish that happiness could always be with you.